UNIVERSIDAD NACIONAL AUTÓNOMA DE MÉXICO
PROGRAMA DE MAESTRÍA Y DOCTORADO EN INGENIERÍA
INGENIERÍA CIVIL — HIDRÁULICA

MODELIZACIÓN INTEGRADA DE FLUJOS SUPERFICIALES Y REDES DE DRENAJE EN UN AMBIENTE URBANO

INTEGRATED MODELLING OF OVERLAND FLOWS AND DRAINAGE NETWORKS IN A URBAN ENVIRONMENT

TESIS
QUE PARA OPTAR POR EL GRADO DE:
DOCTOR EN INGENIERÍA

PRESENTA:
LAURENT GUILLAUME COURTY

TUTOR PRINCIPAL
DR. ADRIÁN PEDROZO ACUÑA, INST. DE INGENIERÍA DE LA UNAM

COMITÉ TUTOR
PROF. PAUL DAVID BATES, SCHOOL OF GEOGRAPHICAL SCIENCES, U. OF BRISTOL
DR. RAMÓN DOMÍNGUEZ MORA, INST. DE INGENIERÍA DE LA UNAM
DR. OSCAR ARTURO FUENTES MARILES, INST. DE INGENIERÍA DE LA UNAM
DR. VICTOR HUGO ALCOCER YAMANAKA, INST. MEXICANO DE TEC. DEL AGUA

CIUDAD DE MÉXICO, MARZO 2018

Presidente: Dr. Ramón Domínguez Mora, Instituto de Ingeniería de la UNAM

Secretario: Dr. Oscar Arturo Fuentes Mariles, Instituto de Ingeniería de la UNAM

1$^{er.}$ Vocal: Dr. Adrián Pedrozo Acuña, Instituto de Ingeniería de la UNAM

2$^{do.}$ Vocal: Dr. Victor Hugo Alcocer Yamanaka, Inst. Mexicano de Tec. del Agua

3$^{er.}$ Vocal: Prof. Paul David Bates, University of Bristol

Lugar o lugares donde se realizó la tesis: Instituto de Ingeniería de la UNAM, Ciudad de México

TUTOR DE TESIS:

Dr. Adrian Pedrozo Acuña

_____

FIRMA

The first 90 percent of the code accounts for the first 90 percent of the development time. The remaining 10 percent of the code accounts for the other 90 percent of the development time.

Tom Cargill, Bell Labs

Resumen

Las inundaciones son ya uno de los desastres más común a nivel global. Con los efectos combinados de la urbanización y el cambio climático, el número de eventos y personas personas afectadas está destinado a aumentar. Por su capacidad de evaluación de múltiples escenarios de clima y desarrollo urbano a un bajo costo, la modelación numérica de inundaciones es una herramienta primordial para hacer frente a estos retos. En las ultimas décadas y como resultado del desarrollo tecnológico, el número de modelos numéricos disponibles se incrementó considerablemente, convirtiéndose en una herramienta indispensable para los ingenieros, las autoridades publicas y los académicos. A pesar de estos avances, la simulación adecuada de los procesos hidrológicos ocurriendo en un ambiente urbano sigue siendo un reto. Dentro de los requerimientos más importantes para que un modelo de inundaciones urbanas se considere adecuado, está la capacidad de resolver los flujos superficiales y en la red de drenaje, así como las interacciones complejas que tienen lugar entre estos dos sistemas. Además, la combinación de las grandes escalas de las ciudades contemporáneas, así como la alta resolución espacial que se necesita para la adecuada representación de los flujos superficiales, redundan en un alto coste computacional, lo que limita su uso en sistemas de predicción avanzados, como las simulaciones probabilistas que hacen uso de ensambles climáticos.

Esta tesis describe la implementación de un nuevo modelo acoplado, que considera la simulación del flujo superficial y la red de drenaje, así como su interacción. Esta herramienta, de código abierto, aprovecha los avances recientes en el campo de hidráulica urbana. El modelo de flujo superficial emplea un esquema numérico simplificado que permite la simulación rápida a alta resolución. Mientras que el modelo de drenaje corresponde a una implementación del famoso software Storm Water Management Model, desarrollado por la Agencia de Protección del Medio

Ambiente de los Estados Unidos de América. La herramienta considera el intercambio de agua entre la superficie y el drenaje por medio de la implementación de ecuaciones de vertedero y orificio determinadas por medio de un modelo físico en laboratorio.

La validación de la parte de flujo superficial de esta herramienta se llevó a cabo a través de la comparación de resultados numéricos contra aquellos derivados de soluciones analíticas de la ecuaciones de aguas someras y de un modelo ampliamente reconocido por al comunidad académica. Para ello también se utilizó información relativa a un caso en la Ciudad de Hull en el Reino Unido. Mientras que para el modelo acoplado se consideró la comparación de los resultados contra aquellos obtenidos por modelos similares en un caso sintético. Por ultimo el modelo completamente acoplado fue utilizado para reproducir la inundación que ocurrió en la ciudad de Kolkata en la India, para la que se tiene información sobre la precipitación, la red de drenaje y algunos niveles de inundación registrados por al policía local. En todos estos casos, el modelo desarrollado da resultados adecuados que otorgan confianza sobre la herramienta y su utilización en el mapeo del riesgo de inundación dentro de ambiente urbanos.

Abstract

Flood is already one of the most common disaster at a global scale. With the combined effects of the continuing urbanization and ongoing climate change, the number of both inundation events and affectees is set to increase. Numerical flood simulation is a key tool to be better prepared to tackle those changes, as it allows us to evaluate the impacts of multiple weather and development scenarios at a reduced cost. In the past decades, flood models have become more reliable and accessible, leading them to be now part of the common toolbox of consulting engineers, public authorities and academics. However, correctly model the hydrological processes occurring in a urban environment is a challenging task. A successful urban flood model should be able to resolve the overland flows, the drainage network flows, and the complex interactions that are taking place between those two systems. Furthermore, the combination of the large scale of modern cities and the fine resolution needed to adequately model the overland flows requires large computational resources, and limits the models usefulness for advanced applications, like ensemble analysis.

The present describes a new, open-source, coupled flood model that takes advantage of recent advances in urban inundation modelling. The surface model of the developed tool employs a simplified numerical scheme that allows fast simulation at high resolution. The drainage network model is the well known Storm Water Management Model, developed by the United States Environmental Protection Agency. The simulation of the coupling between the drainage and the surface models is based on the knowledge recently acquired by physical modelling.

The developed surface model is first evaluated against a combination of analytic solutions and a well-known similar model. It is then employed to the reproduction of an historical flood in the city of Hull, UK. The coupled surface-drainage model is first compared to similar commercial

and academic models. Then, the coupled model is applied to an historical flood in the city of Kolkata, India. In all those tests, the developed software gives adequate results and paves the way to its use for flood risk mapping and drainage network design.

Acknowledgements

First I thank Doctor Adrián Pedrozo Acuña for receiving me in his research group. I am grateful for his constant support and advise. I am in debt of Doctor Luis Álvarez Icaza who, while coordinator of the postgraduate program in engineering at UNAM, helped me to navigate the administrative steps leading to my inscription in the program, and assisted me to receive the financial support needed to carry out that doctorate. I thank the members of my doctoral committee, and especially Professor Paul Bates, for their constructive comments. I acknowledge Prof. Bates for kindly receiving me for an academic stay in his research group at the University of Bristol. I extend my gratitude to Jeff Neal and Mark Trigg who made my stay at the School of Geographical Sciences a productive and pleasant one.

For their friendship and their good mood, I deeply thank all my fellow postgraduate students at the Institute of Engineering. My thoughts goes especially to Alejandra, Juan Pablo, Roberto, Saúl and Roberta. Thank you for all the fun and productive times we had during those years. I also deeply thank my parents for them unshakable support, even during the difficult moments. If it was not for them, I would not be where I am today.

Although I doubt that an endeavour such as a PhD could be successfully concluded without dedicated work, I believe that favourable circumstances are beneficial to even be in a position to consider that degree. Being born a white male in a caring middle class family from a western country certainly helped me in the various career steps that leaded me to where I am now. In that sense, I believe it is right to acknowledge the benefits that I received from those privileges. I humbly wish to be able to promote better equality in my future work places.

Finally, I am grateful to my lovely wife Beatriz. She did not know that she was marrying a future student, but supported me nonetheless during all my doctoral studies. For your love and support, thank you.

Academic production related to this work

Publications in academic journals

- Courty, L. G., A. Pedrozo-Acuña and P. D. Bates (2017). 'Itzï (version 17.1): an open-source, distributed GIS model for dynamic flood simulation'. In: *Geoscientific Model Development* 10.4, pp. 1835–1847. DOI: 10.5194/gmd-10-1835-2017. URL: http://www.geosci-model-dev.net/10/1835/2017/.
- Courty, L. G., M. Á. Rico-Ramirez and A. Pedrozo-Acuña (2018). 'The Significance of the Spatial Variability of Rainfall on the Numerical Simulation of Urban Floods'. In: *Water* 10.2, p. 207. DOI: 10.3390/W10020207. URL: http://www.mdpi.com/264172.

Publications in conference proceedings

- Courty, L. G. and A. Pedrozo-Acuña (2016a). 'A GRASS GIS module for 2D superficial flow simulations'. In: *Proceedings of the 12th International Conference on Hydroinformatics*. DOI: 10.5281/zenodo.159617.
- Courty, L. G. and A. Pedrozo-Acuña (2016b). 'Modelo numérico para la simulación dinámica de inundaciones urbanas en SIG'. in: *Proceedings of XXVII Congreso Latinoamericano de Hidráulica*. DOI: 10.5281/zenodo.159619.

Presentations at conferences and workshops

- 'Flood modelling in mega-cities using a coupled drainage-surface

flow model: Kolkata, India'. International Conference on Urban Drainage. Prague, Czechia. September 2017.

- 'Evaluation of open global Digital Elevation Models for urban flood modelling'. Seventh International Conference on Flood Management. Leeds, UK. September 2017.
- 'The significance of infiltration and spatial variability of rainfall on the numerical reproduction of urban floods'. Seventh International Conference on Flood Management. Leeds, UK. September 2017.
- 'An open-source GIS model for urban floods simulation'. Flood impact assessment in mega cities under urban sprawl and climate change workshop. Orlando, Florida, USA. October 2016.
- 'Modelo numérico para la simulación dinámica de inundaciones urbanas en SIG'. XXVII congreso latinoamericano de hidráulica. Lima, Peru, September 2016.
- 'A GRASS GIS module for 2D superficial flow simulations'. 12th International Conference on Hydroinformatics. Incheon, Republic of Korea. August 2016.

Contents

List of Figures

List of Tables

List of source code listings

List of acronyms

API Application Programming Interface.
CFL Courant–Friedrichs–Lewy.
CSI Critical Success Index.
CSV Comma Separated Values.
DB database.
DEM Digital Elevation Model.
DTM Digital Terrain Model.
EA Environment Agency of the United Kingdom.
EPA United States Environmental Protection Agency.
FCRM Flood and Coastal Risk Management.
FOSS Free and Open Source Software.
GDP Gross Domestic Product.
GIS Geographical Information System.
GLC30 Global Land Cover.
GRASS Geographic Resources Analysis Support System.
HCC Hull City Council.
KED Kriging with External Drift.
LiDAR Light Detection And Ranging.
NSE Nash-Sutcliffe Efficiency.
RMSE Root Mean Square Error.
RSR ratio of the root mean square error to the standard deviation of reference data.
SVE Saint-Venant Equations.
SWE Shallow Water Equations.
SWMM Storm Water Management Model.
USDA United States Department of Agriculture.
ZMVM Metropolitan Area of the Valley of Mexico.

List of symbols

Δt global model time-step [T].
$\Delta t_{\mathbf{1D}}$ time-step of the sewer model [T].
$\Delta t_{\mathbf{2D}}$ time-step of the surface model [T].
$\Delta t_{\mathbf{2D\ max}}$ maximum time-step of the surface model [T].
n Manning's friction [$T/L^{1/3}$].
d water depth[L].
d_f flow depth [L].
$d_{f\,\mathbf{min}}$ minimum flow depth [L].
$d_{\mathbf{max}}$ maximum water depth throughout the raster domain[L].
z ground surface elevation [L].
$z_{\mathbf{crest}}$ node crest elevation [L].
h hydraulic head, equivalent to $z+d$ [L].
$h_{\mathbf{mh}}$ node hydraulic head [L].
$h_{\mathbf{2D}}$ hydraulic head in the surface model [L].
u flow celerity [L/T].
u_r routing celerity [L/T].
q specific flow [L^2/T].
Q volumetric flow [L^3/T].
Q_e raw volumetric flow between surface and drainage [L^3/T].
$Q_{\mathbf{link}}$ adjusted volumetric flow between surface and drainage [L^3/T].
S hydraulic slope [L/L].
t time [T].
g acceleration due to gravity [L/T^2].
α time-step adjustment factor.
θ inertia weighting coefficient.
f infiltration rate [L/T].
F infiltration amount [L].
K soil hydraulic conductivity [L/T].
ϕ_e effective porosity [L/L].
ϕ initial water soil content [L/L].
ψ_f wetting front capillary pressure head [L].
W weir width [L].
$A_{\mathbf{mh}}$ node surface area [L^2].
$A_{\mathbf{cell}}$ node surface area [L^2].
$C_{\mathbf{fw}}$ free weir coefficient.
$C_{\mathbf{sw}}$ submerged weir coefficient.
C_o orifice coefficient.

1 Introduction

Floods were the most common disaster during the last decade, with more than 1700 recorded events between 2006 and 2015 (IFRC, 2016). During the same period, inundations affected 830 000 people, more than any other disaster, killed 57 000 and caused USD 342.7 billion in damage, second only to earthquakes (IFRC, 2016).

According to the United Nations (2014), 54 % of the world's population was living in urban areas in 2014. This ratio is expected to reach 66 % by 2050. By this date, it is estimated that 2.5 billion humans will live in cities. Cities not only concentrate human lives, but also economic and political activities. In 2007, 600 cities where contributing to 60 % of the world Gross Domestic Product (GDP), although hosting only 22 % of the world population (Dobbs et al., 2011). Consequently, urban flooding does generate important disruption to human lives and activities.

With a warmer climate, hydro-meteorological extreme events like floods and droughts will become more frequent. Hirabayashi et al. (2013) predict that floods will become more common by the end of the century, especially in Southeast Asia, India, East Africa and northern Andes. Combining urban growth and higher flood risk, it is logical that the floods that affect urban areas will become more frequent as well. Indeed, Hallegatte et al. (2013) anticipate that the flood-related damages to coastal cities worldwide could reach USD 1000 billion per year in 2050.

In order to better prevent and limit the impacts of urban floods, it is necessary to develop tools that improve our understanding of the processes at work. Numerical models are natural allies in that quest. They allow us to both fill the gap of partial or uncertain field measurements and predict the future (Beven, 2012). However, in the literature there is no single model that is perfect and that can be applied universally. For instance, numerical models only partially represent reality due to the many assumptions that are involved in their development. Those assumptions

have an effect on the reliability of the numerical results produced by the models. It is one of the task of both model designer and modeller to trade off the amount of accuracy required for a specific study and the other variables, such as the necessary computing power. To face the challenge of urban floods that we presented above, it is necessary for the society to have access to numerical models that can represent inundation of cities with an adequate level of complexity. This needs a proper balance of the modelled processes and infrastructures and the ever increasing size of the urban areas to be studied.

1.1 Motivation

1.1.1 Urban floods in Mexico

In 2010, close to 78 % of the population of Mexico was living in cities (INEGI, 2012). Between 2005 and 2010, the urban population in Mexico grew by an average of 3 % a year (INEGI, 2012) In the case of the Metropolitan Area of the Valley of Mexico (ZMVM), that includes Mexico City, the growth was slower than other Mexican metropolis. However, the outer rings of the urbanised area grew by more than 30 % between 2000 and 2010 (Almejo and Téllez, 2015). This evolution denotes a spatial extension of the urban area, increasing both the stress on the existing infrastructure and the detrimental effects of the urbanisation on the hydrologic cycle (Kishtawal et al., 2010; Miller et al., 2014).

Especially, the ZMVM is concentrating several challenges inherent to its geographical situation. Most of its constructed area is located in an endorheic lake bed; there is no natural outlet for rainwater. Therefore, most of the run-off water need to be transported out of the valley by large, dedicated infrastructures (García Cortés and Hernández Serrano, 1975; Ríos Elizondo et al., 1975). Additionally, the combined effect of soil imperviousness and excessive extraction of groundwater lead to land subsidence up to 40 cm per year (Hernández-Espriú et al., 2014). This land subsidence has in turn adverse impacts on the drainage infrastructure, from damages caused by differential sinking to loss of capacity due to reduced or even inverted gradient (Ríos Elizondo et al., 1975).

It is therefore no surprise that urban floods are a common problem for dwellers of Mexico City. Even though no major inundation occurred since the great flood of 1951 (Páramo, 2014), significant events that disturb

the city life are expected during every rainy season (e.g. Animal Político, 2016, 2017). The direct material damages of those events are usually limited, but those regular disruptions of public services and transportations are inducing important indirect costs, although their actual estimation might be challenging (Domínguez-Mora, 2000).

1.1.2 Geographical Information System

Geographical Information System (GIS) are indispensable tools for hydrologists nowadays. Indeed, geographical information, from DEM to observation data, is central to earth sciences in general. It therefore makes sense to possess tools that permit the manipulation and analysis of those geographical data. The use of GIS for the manipulation of remote sensing data is quite established, and the advent of web mapping made GIS more ubiquitous. Therefore, there have been efforts for decades to integrate hydrological models with GIS. That integration could be classified as tight or loose. A tight integration would mean that the model is integrated inside the GIS, by the use of the software Application Programming Interface (API) to interact with the geographical data from the spatial database. A loose integration consists usually of a model accepting GIS file formats as inputs, and returning the results in a format that could be imported or visualised in the GIS. While some commercial software do feature a tight coupling (usually with a proprietary GIS software like ArcGIS), academic flood models are more commonly loosely coupled. LISFLOOD-FP (Bates and De Roo, 2000) is an example of loosely coupled academic flood model. Tightly integrated models make it easier to take advantage of some of the GIS spatial tools, and prevent the need of exporting model input maps and importing the modelling results back into the GIS.

1.1.3 Free software

Free software and open-source software have slightly different definitions (Free Software Fundation, 2016; Open Source Initiative, 2007), but they share some core principles. That is why they are sometimes grouped under the term of Free and Open Source Software (FOSS). Notably, they both allow the freedom of using, modifying and distributing a software without restriction. This has several advantages over proprietary software.

First, using this type of software eliminates license costs and the burden it implies (hardware dongle, license server etc.). This is a great asset for research and teaching institutions as well as government agencies for which the licensing cost might too high, especially in the developing world where financial resources are scant. In the case of higher education, some universities might provide free or discounted software licenses for their students, but it is not a generalized practice. Therefore, teaching proprietary software might incite students to illegally install unlicensed products on their computer to complete a coursework. Apart from the legal risk, this practice is arguably at odds with the academic principles of integrity and respect of intellectual property.

Second, the publication of the source code greatly simplify the reproducibility of researches. Although many scientific articles in computational hydraulics do provide some insight about the main equations that they employ, detailed description of the software implementation of the algorithm is seldom integrated. Even though a complete description is provided in an article, writing an entirely new software to reproduce the results of a scientific paper might rightfully be considered as an unnecessary burden. Having access to the software used to produce the published is a principle of open science and a step in the direction of resolving the current reproducibility crisis that affects the science community (Baker, 2016).

Third, not only using FOSS lower the barrier to reproducibility, it also reduce the development time of new software. Building upon a previous work is a fundamental principle of both scientific and FOSS practices. One successful example in the hydroinformatics community is the Storm Water Management Model (SWMM), released by the United States Environmental Protection Agency (EPA) as a public domain software. It has been used as a base for both commercial softwares (e.g. XPSWMM, InfoSWMM, PCSWMM) and scientific works (e.g. Hsu et al., 2000; Leandro and Martins, 2016; Seyoum et al., 2012) Having a strong, widely accepted software base helps to prevent the development time spent to reinvent the wheel. Scientists can then focus their limited time to write the innovative piece of software necessary for their research.

Harvey and Han (2002) identified that the FOSS have great potential in the hydroinformatics community. Since then, various FOSS projects related or applicable to the hydroinformatics have been released. They range from building blocks that ease software development (e.g. Pedre-

gosa et al., 2011; Van Der Walt et al., 2011) to desktop GIS (e.g. QGIS[1]) and flow modelling packages (for example FullSWOF (Delestre et al., 2014) or ANUGA (Mungkasi and Roberts, 2013)). The FOSS community is indeed thriving and the popularity of online collaborations tools like github[2] is both a testimony and a catalyst of the FOSS development in the recent years.

The lower licensing and legal burden, better understanding of algorithm implementations and possibility to build upon the work of others are all assets for the use of FOSS in higher education. Indeed, FOSS have been successfully integrated in university courses (Mitášová et al., 2012; O'Hara and Kay, 2003).

1.2 Objectives

1.2.1 Main objective

This work aims at developing a free software tool that permits the coupled modeling of urban floods.

1.2.2 Specific goals

The specific goals that support the accomplishment of the main objective are as follow:

1. Develop a surface model that implement an explicit, partial inertia numerical scheme.
2. Integrate that surface model within an open-source GIS.
3. Implement a bi-directional coupling of the surface model with a drainage network model.
4. Test, validate and apply the newly-developed software to various test cases.
5. Distribute the software under an open-source license.

[1] https://qgis.org
[2] https://github.com/

1.3 Thesis structure

This thesis is organized in three principal chapters. Chapter 2 presents a review of related works. Chapter 3 describes the structure of developed software and is divided in two Sections; one related to the surface flow model and other to the coupling mechanism. Finally, two case studies are presented in Chapter 4; one that uses the overland flow model alone, and one using the coupled model.

2 State of the art

2.1 Surface modelling using simplified explicit formula

The state of the art in surface flow modelling is the use of the two-dimensional Shallow Water Equations (SWE). However, the computational cost of the numerical resolution of these equations is high, especially at the high resolution that is required for urban flood modelling. Hence, the flood modelling community sought simplifications of this equation system that would allow both an adequate representation of the real world processes, and a reasonable computational time. Since the work of Bates and De Roo (2000), many other authors used a diffusive wave formula on regular raster grid to simulate flood plain inundation (e.g. Bradbrook et al., 2004; A. S. Chen et al., 2005; Jahanbazi et al., 2017; Seyoum et al., 2012; Yu and Lane, 2006). This popularity might be due to its ease of implementation and the relative low computation needs compared to the SWE when using a coarse resolution. However, in order to maintain stability with lower cell sizes, this type of numerical scheme require very small time-steps, to a point where it could be slower than the SWE (N. M. Hunter et al., 2008; Neal et al., 2012). This limits the interest of such models in urban areas where high spatial resolution is needed to represent urban features (Fewtrell et al., 2011). The parallelization of such model (Leandro et al., 2014; Neal et al., 2010) does not overcome those limitations which are inherent to the simplified formulation. In addition to that performance problem, it is controversial whether the diffusive wave approximation is well adapted to urban floods where flows are complex (Costabile et al., 2017).

An step forward was made by Bates et al. (2010) that developed a new explicit formula that includes the acceleration term of the one-

dimensional Saint-Venant Equations (SVE), neglecting the advection. This formula proved to be orders of magnitude faster than non-inertia formulas for DEM with higher spatial resolution (Bates et al., 2010; Neal et al., 2012). However, the authors noticed that this numerical scheme suffers from instabilities at low friction. Whilst the utility of this formula for the flood modelling of urban catchments has been demonstrated (Neal et al., 2011; Yu and Coulthard, 2015), the occurrence of instabilities at low frictions could be seen as a limitation in urban areas where smooth surfaces are common. This identified limitation motivated follow-up studies (Almeida and Bates, 2013; Almeida et al., 2012) that worked on improving the formula from Bates et al. (2010) by integrating both an inertia damping and a bi-dimensional friction term. The authors found that this new formulation allows a better stability under conditions of lower roughness coefficient.

Despite those advances, simplified explicit formulas are not well adapted to supercritical flows. Those flows regimes usually happen in terrains with steep slopes. This is problematic for the use of direct rainfall, that will occur on every part of the computational domain. Different solutions to that issue are described in the literature. Sampson et al. (2013) presented a simplified routing scheme which is triggered when the water depth is below a user-defined threshold (proposed to be equal to 5 mm). The water is then routed at a constant velocity (set to 0.1 by default) along a direction determined by the topography alone. Sampson et al. (2015) uses a rain-routing technique inspired by the work of Sampson et al. (2013). However, in that case the hydraulic slope is used as a threshold instead of the water depth. Then, the flow velocity is calculating depending on the surface gradient. It is not clear however which exact formula is used by the authors, as the work they cite as a reference (Kent et al., 2010) presents different methods to evaluate the surface velocity. Finally, Adams et al. (2017) developed a Python library that simulates overland flows using the damped simple inertia numerical scheme presented by Almeida et al. (2012). The stability condition they use is based on the Froude number. Their code adjusts the velocity of the flow so that the Froude number is limited to a maximum of 1. The authors consider it as an acceptable approximation based on the work of Grant (1997). The latter found via field observations that flows in mountainous streams seldom reach a Froude number above 1 over long distances.

2.2 Drainage-surface coupled modelling

If resolving the surface flow is obviously necessary to represent urban floods, it is by no mean sufficient. To prevent inundations and diseases, Humans created drainage networks for thousands of years (Chocat et al., 2001). It is therefore logical to integrate in a urban inundation model the very infrastructure that is designed to reduce the floods. As a consequence, this subject has been of strong interest in the last decades.

Historically, modelling software packages for urban drainage networks were developed first, due to the lower hardware requirements compared to 2D surface flow models. For example, the popular models SWMM and MOUSE have been first published in 1970 and 1983, respectively (Elliott and Trowsdale, 2007). In the 1990's, interest in the combined modelling of surface and drainage network grew, with the development of the concept of dual-drainage (e.g. Pankratz et al., 1995). However, those first iterations where coarse; the overland routing was represented with simplistic formulas and the interaction between the drainage and the surface was a direct mass exchange. Later, Djordjević et al. (1999) presented an improved paradigm of dual-drainage, where the street above the drainage system is represented as another kind of unidimensional network, resolved with the same equations. In this system, the interactions between the the drainage and the surface are bidirectional, allowing the sewer to drain the street and to overflow to the surface (Leandro et al., 2007). Despite the demonstrated capacities of this one-dimensional dual-drainage procedure to reproduce urban floods, much care need to be applied to calibration and identification of the overland flow patterns (Leandro et al., 2009; Mark et al., 2004; Vojinovic and Tutulic, 2009).

With the improvement of computer hardware, the coupling of 2D surface models with unidimensional drainage became possible, encouraging the development of this type of models (e.g. Hsu et al., 2000; Schmitt et al., 2004, 2005). However, those first iterations were having a simplistic view of the hydraulic processes occurring at a linking node, considering that the surcharge of a drainage node was inducing a complete transfer of the overflow volume from the drainage network to the overland model. Therefore, some authors proposed to use a combination of weir and orifice equations to estimate the interchange flows (Carr and G. Smith, 2007; A. S. Chen et al., 2007). This last approach has proved to be popular and a range of implementation has been published. Table 2.1 presents a comparison of selected literature using a combination of weir

and orifice equation to model the bidirectional transfer of mass between the drainage and the overland flow model.

However, the correct application of those equations requires the determination of weir and orifice coefficients. Indeed, it is well known that a storm water inlet seldom functions at its design capacity (e.g. Aronica and Lanza, 2005; Leitão et al., 2017; Palla et al., 2016; Senior et al., 2018). To reduce the related uncertainties, some authors carried out a combination of physical and 3D numerical simulations (Djordjević et al., 2011; Lopes et al., 2013). While 3D models provide a better physical description of the flow, their implementation is more computationally intensive than 2D models, which make difficult their usability in practical problems. The comparison of the result of a coupled 1D/2D model with an experimental model showed that this numerical modelling is indeed robust (Bazin et al., 2014; Fraga et al., 2017). Although Fraga et al. (2017) employ a model using the combination of weir and orifices presented by A. S. Chen et al. (2007), they fall short of indicating the weir and orifice coefficient used in their model. This issue has been addressed by Rubinato et al. (2017) that compared a scaled physical model of a surface/sewer system and compared the measurements with the results of a numerical model implementing a weir/orifice-based interface. This permitted the authors to propose weir and orifice coefficients to be used by models using this type of interface. This however should be considered a first step, as some preliminary results obtained with a similar physical set-up that allows the change in slope of the flume indicates that those coefficients might be correlated with the Froude number of the overland flow (Hakiel and Szydłowski, 2017).

Table 2.1: Comparison of surface–drainage coupling interfaces using a combination of weir and orifice equations.

Reference	Surface Model	Drainage model(s)	Sewer to surface	Surface to sewer
A. S. Chen et al. (2007)	Diffusive (UIM)	SIPSON	FW, SW, O	FW, SW, O
Seyoum et al. (2012)	Diffusive	SWMM	FW, SW, O	FW, SW, O
A. S. Chen et al. (2015)	Diffusive (P-DWave)	SIPSON	O	SW, O
Leandro and Martins (2016)	Diffusive (P-DWave)	SIPSON and SWMM	O	SW, O
Rubinato et al. (2017)	SWE	Unknown	O	FW, SW, O
Martins et al. (2017)	SWE, Diffusive wave and partial inertia	SIPSON	O	SW, O
This work	Partial inertia	SWMM	O	FW, SW, O

FW: free weir. SW: submerged weir. O: orifice.

3 Description of the developed software

This Chapter details the developed framework along with its implementation and integration. The resulting software is called Itzï, after the Purépecha word for 'water'. Itzï integrates a newly written partial inertia surface model with the SWMM drainage model. The software is build upon the open-source GIS Geographic Resources Analysis Support System (GRASS) (Neteler et al., 2012), that it uses for reading input maps and writting resulting data. Figure 3.1 shows the architecture of the developed tool.

Section 3.1 describes the numerical scheme and the software implementation of the surface model, while Section 3.2 explains how the overland flow model is coupled with the SWMM drainage model.

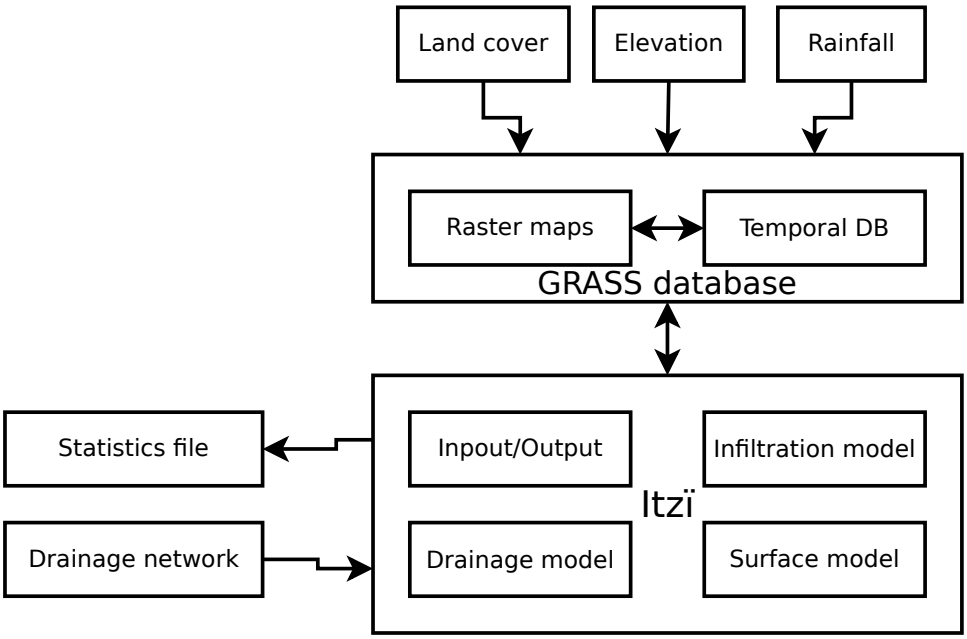

Figure 3.1: Organization of the proposed architecture.

3.1 Overland flow model

This Section has been published as:

> Courty, L. G., A. Pedrozo-Acuña and P. D. Bates (2017). 'Itzï (version 17.1): an open-source, distributed GIS model for dynamic flood simulation'. In: *Geoscientific Model Development* 10.4, pp. 1835–1847. DOI: 10.5194/gmd-10-1835-2017. URL: http://www.geosci-model-dev.net/10/1835/2017/.

3.1.1 Numerical scheme

The developed program uses an explicit finite-difference scheme to solve the simplified partial inertia shallow-water equations described by Almeida et al. (2012) and Almeida and Bates (2013). Figure 3.2 illustrates the variables used by the scheme in the x dimension and their variations in time. On the other hand Fig. 3.3 introduces a complete 2D view of the same staggered grid and variables utilised in the numerical scheme. As

shown in Fig. 3.2, water surface elevation h and water depth d are evaluated in the centre of cells, while the water flow q (or celerity u) variables are evaluated at the cell interfaces.

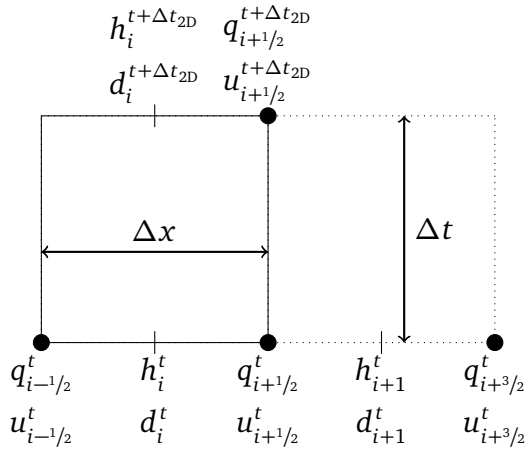

Figure 3.2: Grid and variables used in the numerical scheme.

The mass flux (e.g. water flow) is obtained by solving the one-dimensional simplified momentum equation at interfaces between cells using the value of q at these interfaces (rather than in the centre of cells). To provide a bidimensional representation of the flow, momentum itself is updated at the cell interfaces with an explicit discretization of the momentum equation in each direction separately. The numerical method is simple and extremely efficient from a computational point of view. For simplicity, in this section we will present only the flow equation for the x dimension. The exact same principle applies for water flows in the other direction, which is represented by the y dimension.

3.1.1.1 Adaptive time-step

In a similar vein to previous developments, an adaptive time stepping method is used to estimate the suitable model time step based on the standard Courant–Friedrichs–Lewy (CFL) condition. The time-step Δt_{2D} is calculated at each time-step by means of Equation 3.1.

$$\Delta t_{2D} = \alpha \frac{\min\{\Delta x, \Delta y\}}{\sqrt{g \times d_{\max}}} \tag{3.1}$$

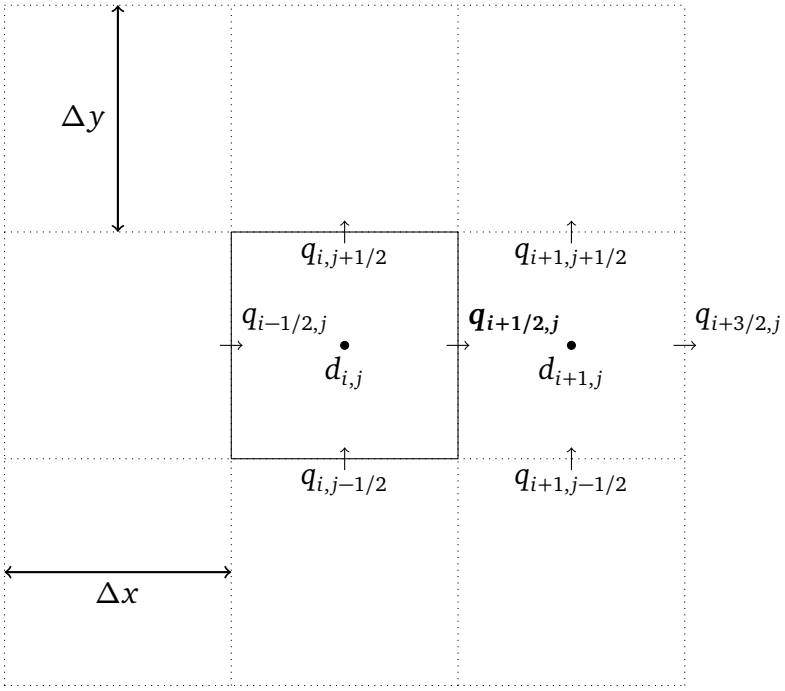

Figure 3.3: A 2D view of the staggered grid used by the numerical scheme.

Where $d_{\max}$ is the maximum water depth within the domain, g the acceleration due to the gravity and α an adjustment factor because the CFL condition is necessary but not sufficient to ensure stability. Almeida et al. (2012) propose a value of $\alpha = 0.7$ as a default, as this has been shown to allow the appropriate simulation of subcritical flooding conditions. When $d_{\max}$ tends to 0, Δt_{2D} is set to a user-defined time-step $\Delta t_{2D\,\max}$, which represents the maximum value for Δt_{2D}. Here the default for this value has been set to 5 s. It could be adjusted by the user to optimize computation time while preserving numerical stability.

3.1.1.2 Flow calculation

The flow at each cell interface is calculated with Equation 3.2.

$$q_{i+1/2}^{t+\Delta t_{2D}} = \frac{\left(\theta q_{i+1/2}^{t} + (1-\theta)\frac{q_{i-1/2}^{t} + q_{i+3/2}^{t}}{2}\right) + g d_f \Delta t_{2D} S}{1 + g\Delta t_{2D} n^2 \|q_{i+1/2}^{t}\| / {d_f}^{7/3}} \tag{3.2}$$

where subscripts i and t denotes space and time indices (See Fig. 3.2).

The flow depth d_f is the difference between the highest water surface elevation h and the highest terrain elevation z. It is calculated at the cell face using Equation 3.3. This value is used as an approximation of the hydraulic radius.

θ is a coefficient defining the importance taken by the average of upstream and downstream flows over the flow at the considered cell face ($q_{i+1/2}^{t}$). Almeida et al. (2012) propose to set this weighting factor to 0.9. If θ is set to 1, neighbouring flows are not taken into account, being equivalent to the formula proposed by Bates et al. (2010). In some rare cases, especially when θ is low, the flow term could end up with a different sign to the slope term. When this happens, the weighting scheme is dropped and the numerator of the equation becomes equal to the formulation presented by Bates et al. (2010).

The slope S is calculated using Equation 3.4. The flow being calculated at cell interfaces, Manning's n is obtained by averaging the neighbouring values, as shown in Equation 3.5.

$${d_f}_{i+1/2}^{t} = \max\left\{h_i^t, h_{i+1}^t\right\} - \max\left\{z_i^t, z_{i+1}^t\right\} \tag{3.3}$$

$$S = \frac{h_i^t - h_{i+1}^t}{\Delta x} \tag{3.4}$$

$$n_{i+1/2}^{t} = \frac{\left(n_i^t + n_{i+1}^t\right)}{2} \tag{3.5}$$

The vector norm $\|q_{i+1/2}^{t}\|$ is calculated using Equation 3.6 given by Almeida and Bates (2013).

$$\|q_{i+1/2}^{t}\| = \sqrt{\left(q_{y,i+1/2,j}^{t}\right)^2 + \left(q_{x,i+1/2,j}^{t}\right)^2} \tag{3.6}$$

Inconveniently, due to the use of a staggered grid, $q_{y,i+1/2,j}^{t}$ is not being calculated by the model. To overcome this, the value of the neighbouring

cells are used instead as shown in Equation 3.7. The positions of the given points are showed on Fig. 3.3.

$$q^t_{y,i+1/2,j} = \frac{q_{i,j-1/2} + q_{i,j+1/2} + q_{i+1,j-1/2} + q_{i+1,j+1/2}}{4} \tag{3.7}$$

The specific flow q in $\mathrm{m\,s^{-2}}$ obtained by Equation 3.2 is converted to $\mathrm{m^3\,s^{-1}}$ using Equation 3.8:

$$Q_i = q_i \times \Delta y \tag{3.8}$$

3.1.1.3 Water depth calculation

The new water depth at each cell is calculated using Equation 3.9. It consists of the sum of the current depth d^t, the external terms (rainfall, infiltration, user-defined flow etc.) d^t_{ext} and the flows passing through the four faces of each cell. If the new calculated water depth is negative,the depth is set to zero. This additional volume is registered and used to estimate of the numerical stability of the model (see Section 3.1.2).

$$d^{t+\Delta t_{2D}} = d^t + d^t_{ext} + \frac{\sum^4 Q^t_{i,j}}{\Delta x \Delta y} \times \Delta t_{2D} \tag{3.9}$$

3.1.1.4 Rain routing

In order to maintain stability during events with direct rainfall, a rain routing mechanism is implemented using a simple method described by Sampson et al. (2013). It consists of applying a constant velocity to the flow when water depth is below a user-given threshold. Before the simulation begins, the software calculates the draining direction of each cell of the domain. The drainage direction is determined by the highest slope out of the four neighbouring cells. During the simulation, the routing scheme is applied at each cell interface when each of the following conditions are true:

- $d_f < d_{f\min}$,
- the considered direction is allowed for routing according to the routing map,
- the slope S is in the same direction as the above routing direction.

The routing flow is then calculated using a constant user-given velocity with Equation 3.10. According to Sampson et al. (2013), a depth

threshold $d_{f\,\min}$ of 5 mm and a routing celerity u_r of 0.1 m s^{-1} gives good results.

$$\Delta d = \min\{(h_i^t - h_{i+1}^t), d_i^t\} \tag{3.10a}$$

$$q_{max} = \Delta x \times \Delta d / \Delta t_{2\mathrm{D}} \tag{3.10b}$$

$$q_{i+1/2}^t = \min\{(u_r \times \Delta d), q_{max}\} \tag{3.10c}$$

3.1.1.5 Infiltration

User-defined rate

In *Itzï*, the infiltration could be represented by a map or a time-series of map containing a fixed-value for infiltration rate in mm h^{-1}. The infiltration model then simply consists in making sure that the actual infiltration is limited to the amount of water ponding above the considered cell.

Green–Ampt method

First presented by Heber Green and Ampt (1911), this widely used method is implemented in Itzï using the formulation in Rawls et al. (1983). The latter is shown in Equation 3.11, where f is the infiltration rate (mm h^{-1}), K the hydraulic conductivity (mm s^{-1}), ϕ_e the effective porosity in (m m^{-1}), ϕ the initial water soil content (m m^{-1}), ψ_f the wetting front capillary pressure head (m) and F the infiltration amount (m).

$$f = K\left(1 + \frac{(\phi_e - \phi)\psi_f}{F}\right) \tag{3.11}$$

3.1.2 Implementation

The software is written in the Python programming language and integrates tightly with the open-source GIS GRASS (Neteler et al., 2012). It employs the libraries *PyGRASS* (Zambelli et al., 2013) to access the geographical functions and *TGRASS* (Gebbert and Pebesma, 2014) for the temporal management of both the input and the output data. Additionally, further optimisation of the numerical code was carried out by means of a Python profiler that records the call stack of the executing code, thus accounting for the time spent in the solution of each function within the code. This enabled the parallelisation through Cython (Behnel et al.,

2011) of those functions with the highest computational cost, reducing the overall computing time by taking advantage of multi-cores CPU. The integration of this numerical model within GRASS provides *Itzï* with the following relevant characteristics:

- The spatio-temporal data management is straightforward as the integration within a GIS platform reduces the time spent on preparation of entry data and the analysis of results. Modifying the spatial extent and resolution of the simulation is done by simply changing the GRASS computational region, without the need for changing the entry data.
- Forcings could be of heterogeneous resolutions. For example elevation at 5 m, rainfall at 1 km, friction coefficient at 30 m etc. *Itzï* will automatically read the data at the resolution defined by the computational region and uses the data seamlessly, without user intervention.
- Input data can vary in space and time (i.e. raster time-series); permitting the use of, for example, spatially distributed rainfall or time-varying friction coefficients.
- The ability to use absolute time references in form of date and time for start and end of the simulation, facilitating the usage of historical rainfall. It is therefore possible to have several years of rainfall data stored in the GIS and to simulate just one specific event, without further data pre-processing.

Itzï is operated by a command line interface taking a parameters file as an input. If several input files are given, they are run in batch mode. The user can ask the software to output the following raster time-series:

- Water depth (d) and surface elevation (h),
- flow velocity magnitude and direction,
- volumetric flows in x and y directions,
- average volume added or subtracted to the domain by the action of infiltration, rainfall, user-defined inflow, drainage capacity or the application of boundary conditions,
- volume created due to numerical instability (See Sect. 3.1.1.3).

Additionally, the software can produce a Comma Separated Values (CSV) file that summarizes the statistics mentioned above.

3.1.3 Verification and evaluation

3.1.3.1 Analytic test cases

For the analytic test cases, we utilise numerical experiments aimed at testing subcritical flow simulations recently published in a compilation of shallow water analytic solutions for hydraulic and environmental studies (Delestre et al., 2013). Both cases described here are constituted by a 1 km long channel of MacDonald's type (MacDonald et al., 1997), discretized at 5 m resolution. These test cases were generated with the free software SWASHES[1].

The first case corresponds to a constant upstream flow of $2\,m^2\,s^{-1}$, while the second one combines an upstream flow of $1\,m^2\,s^{-1}$ and a uniform rainfall with an intensity of $0.001\,m\,s^{-1}$. In the model, the input flow is given as a mass addition. This creates an artificially high water level at the most upstream cell, where the input flow is added. Given that the goal of the analytic tests is to verify the validity of the numerical scheme, we determine the Root Mean Square Error (RMSE) omitting the very first cell of the domain. Figure 3.4 illustrate the performance of *Itzï* at reproducing results from the analytic solution, reporting RMSE of 0.002 and 0.03 metres, for each case respectively. Those RMSE values are one to two orders of magnitudes lower than the vertical accuracy of airborne Light Detection And Ranging (LiDAR) (Hodgson and Bresnahan, 2004), demonstrating the suitability of the implemented simplified scheme to simulate subcritical flow conditions.

3.1.3.2 Direct rainfall and sewer overflow in an urban setting

In order to further test the numerical model, previously published benchmark test cases for 2D flood inundation modelling tools by the Environment Agency of the United Kingdom (EA) (Néelz and Pender, 2013), were implemented. These cases correspond to a benchmarking exercise assessing the latest generation of 2D hydraulic modelling tools for a variety of purposes in Flood and Coastal Risk Management (FCRM) to support EA decision making. This dataset is available online on the EA website[2].

In particular, one hypothetical test case was utilised to verify the proper implementation of the numerical scheme to simulate physical processes

[1] `https://sourcesup.renater.fr/projects/swashes/`

[2] `http://evidence.environment-agency.gov.uk/FCERM/Libraries/FCERM_Project_Documents/Benchmarking_Model_Data.sflb.ashx`

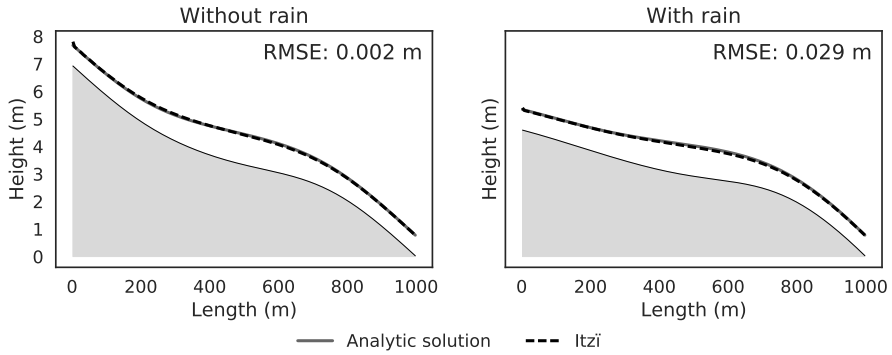

Figure 3.4: One-dimensional MacDonald long-channel.

controlling flood movement across a floodplain. The test case (test case number 8a in the EA study) corresponds to a synthetic event which does not relate to any real event (Néelz and Pender, 2013). The modelled area is in the City of Glasgow, UK (Cockenzie Street and surrounding streets) and is approximately 400 by 960 metres. Ground elevations span a range of 21 m to 37 m. While the flood is assumed to arise from two sources: a uniformly distributed rainfall (applied only to the modelled area) and a point inflow representing a sewer outflow from a surcharging culvert. For completeness, Fig. 3.5 shows both forcings described by the hyetograph and the hydrograph specified at the point inflow. The DEM has a spatial resolution of 0.5m, which is resampled to 2m resolution for modelling purposes. This represents the terrain model with no vegetation or buildings and was created from a LiDAR dataset provided by the EA. The roughness coefficient was determined following the classification of the area with two land-cover roughnesses: roads and pavements ($0.02\,\mathrm{s\,m^{-1/3}}$), and everywhere else ($0.05\,\mathrm{s\,m^{-1/3}}$). The model was run until time $\mathrm{t} = 83$ min as this was considered enough to allow the flood to pond in the lower parts of the modelled domain.

Numerical results obtained with *Itzï* have been compared to those obtained with the implementation of the *acceleration* solver from LISFLOOD-FP (Almeida and Bates, 2013; Almeida et al., 2012). This is done as the latter is considered the reference implementation of the numerical scheme here employed. For this comparison eight different locations within the numerical domain were selected to compare water depths es-

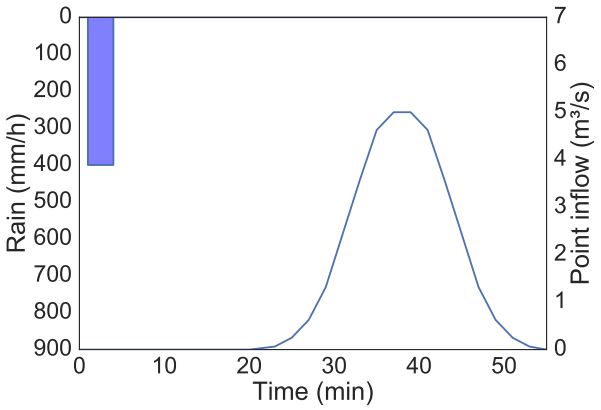

Figure 3.5: Rectangular hyetograph and point inflow hydrograph for the EA test 8a.

timated by both numerical tools. Figure 3.6 illustrates the utilised digital elevation model, along with the position of the inflow point and selected control points for the comparison of model results.

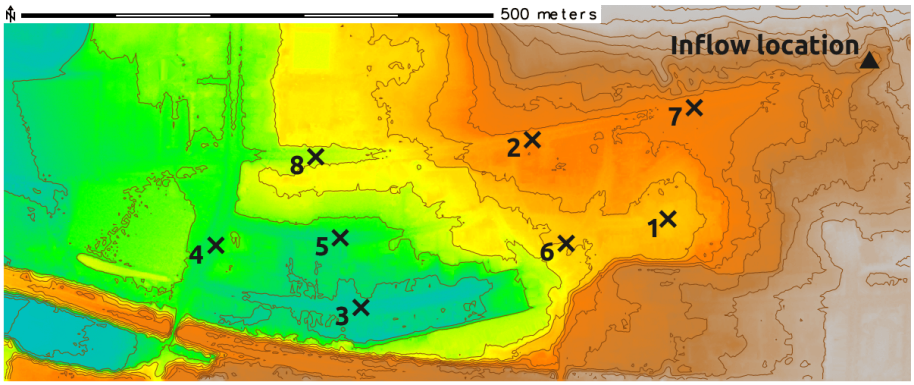

Figure 3.6: DEM of EA test 8a showing the numbered control points (crosses) and inflow point (triangle).

The simulation is run for 83 minutes with both LISFLOOD-FP and *Itzï* using the same parameters, shown in Table 3.1. Figure 3.7 illustrates the time series of water level produced by both numerical models and at the eight selected locations, as well as the time series of differences between the results of the two models. It is shown that in all eight selected locations, numerical results from both models are similar with small differences identified at the arrival time of the flood wave in each location.

These differences are ascribed to the way that LISLFLOOD-FP handles entry data in comparison to *Itzï*. In the first case, a temporal interpolation is performed during the simulation at each time-step, while in the second case, this process should be carried out during the preparation of input space-time raster datasets. The RMSE at the eight location range from 0.2 to 10.6 mm (See Fig. 3.7). This indicates that the numerical solution of the partial inertia approximation implemented in *Itzï* generates results with the same level of skill as the reference model.

Table 3.1: Simulation parameters for the EA test case 8a

Parameter	Value
$\Delta t_{2\mathrm{D\,max}}$	5 s
α	0.7
θ	0.7
u_r	0.1 m s^{-1}
$d_{f\,\mathrm{min}}$	0.005 m

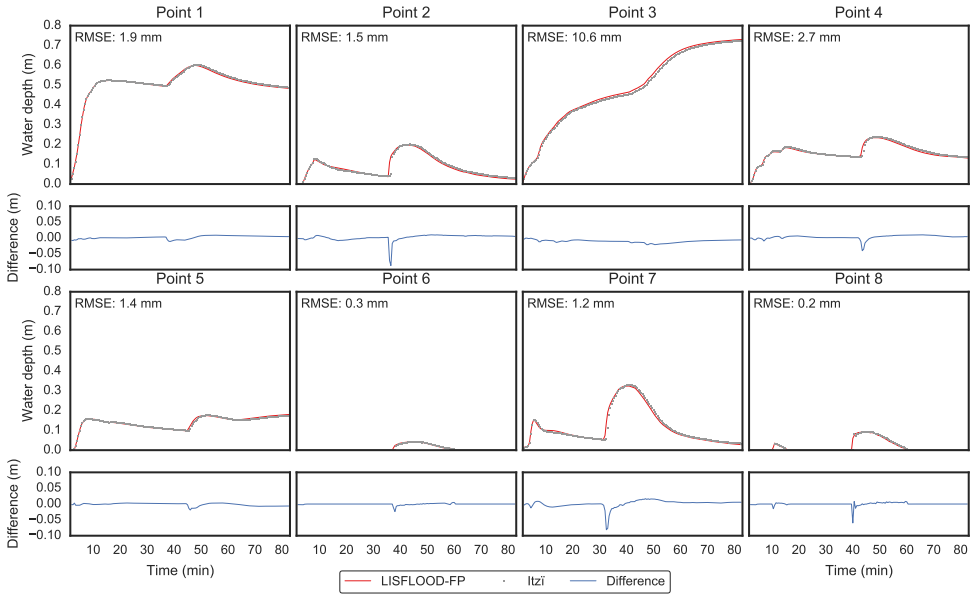

Figure 3.7: Comparison of water depths at control points. The blue line represents the differences of water depth between *Itzï* and LISLOOD-FP.

3.2 Drainage model coupling

This Section is dedicated to the description of the steps taken to couple the SWMM drainage model to the surface model described earlier. Then, the model is validated through the comparison of its results with similar commercial and academic models.

3.2.1 Presentation of Storm Water Management Model

The SWMM has been developed by the EPA to model drainage networks, including: (Rossman, 2010)

- Rainfall-runoff simulation, including precipitation, infiltration, evaporation and snowmelt.
- Flows inside the drainage network using the completes equations of Saint-Venant (1871), i.e. dynamic wave.
- Pollutant transports.
- Special networks elements like tanks, reservoirs, pumping stations, flow dividers etc.

SWMM is a software of reference in urban drainage modelling and it is used by various actors around the world (Leandro and Martins, 2016; Paz et al., 2011; Rossman, 2010; Seyoum et al., 2012; Zhao et al., 2008). The SWMM computational engine is public domain and written in the C programming language. In this study, the developed 2D model (cf. Chapter 3.1) will act as a rainfall-runoff module. Itzï is therefore designed to use SWMM only as a flow routing model. However, Itzï is not preventing the user to run a SWMM model that includes catchments.

3.2.2 Theory of surface-drainage coupling

3.2.2.1 Temporal synchronisation

Temporal synchronisation ensures that the mass exchange between the two models is done at the same simulation time. Itzï is composed of several modules that advances each at a specific time step:

- The infiltration model uses a fixed time-step (default to 60 seconds).
- The module that manages writing results, uses a user-defined time-step.
- The drainage model can use either a fixed or adaptive time-step.
- The overland flow model uses a dynamic time-step.

The solution used is to shorten the time-step duration of the overland flow model to match the next time-step of other model. The adjustment is represented in Equation 3.12, where Δt is the general model time-step, Δt_{2D} is the surface model time-step, t the current simulation time, Δt_{1D} the drainage time-step and Δt_{inf} the infiltration time-step. Only the surface model is run at each general time-step. The other models are run for one step if the current general simulation time is equal to their designated time-step.

$$\Delta t = \min\{(t + \Delta t_{2D}), (t + \Delta t_{1D}), (t + \Delta t_{inf}) \dots\} - t \tag{3.12a}$$

$$\Delta t_{2D} = \Delta t \tag{3.12b}$$

3.2.2.2 Mass exchange

A. S. Chen et al. (2007) propose to calculate the flow interchange between the two models by using weir or orifice equations. This solution has been use by other authors (A. S. Chen et al., 2015; Leandro and Martins, 2016; Martins et al., 2017; Seyoum et al., 2012). Its ability to adequately reproduce actual physical processes has been proven by comparing by physical experiments (Hakiel and Szydłowski, 2017; Rubinato et al., 2017). As seen in Section 2.2, different authors use different combinations of criteria to apply those equations. Itzï employs the scheme used by (Rubinato et al., 2017), because it has been experimentally proven in multiple flow conditions. This scheme combines two weir equations and the orifice equation in case of drainage into the sewer network, and orifice only when the node is overflowing. The following possible cases are recapitulated below:

1. No linkage if both water level inside the node and above ground is below the crest elevation of the node.
2. Orifice equation if $h_{\text{mh}} > h_{2D}$ or $(h_{2D} - z_{\text{crest}}) \geq (A_{\text{mh}}/W)$. This means that when the drainage is overflowing, only the orifice equation is used.
3. Free weir equation if $h_{2D} > z_{\text{crest}} > h_{\text{mh}}$.
4. Submerged weir equation if both water levels are above z_{crest} and $(h_{2D} - z_{\text{crest}}) < (A_{\text{mh}}/W)$.

Where z_{crest} is the elevation of the node's crest, h_{mh} the water elevation in the considered node and h_{2D} the water elevation in the surface model. The different flow equations are shown in (3.13):

$$Q = \begin{cases} C_{\text{fw}} W d_f^{3/2} \sqrt{2g}, & \text{if } h_{\text{2D}} > z_{\text{crest}} > h_{\text{mh}} \\ C_{\text{sw}} W d_f \sqrt{2g(h_u - h_d)}, & \text{if } [(h_{\text{2D}} - z_{\text{crest}}) < (A_{\text{mh}}/W)] \wedge (h_{\text{2D}} > h_{\text{mh}}) \wedge (z_{\text{crest}} > h_{\text{mh}}) \\ C_o A_{\text{mh}} \sqrt{2g(h_u - h_d)}, & \text{if } (h_{\text{mh}} > h_{\text{2D}}) \vee [(h_{\text{2D}} - z_{\text{crest}}) \geq (A_{\text{mh}}/W)] \end{cases} \tag{3.13}$$

with

$$h_u = \max\{h_{\text{mh}}, h_{\text{2D}}\} \tag{3.14a}$$

$$h_d = \min\{h_{\text{mh}}, h_{\text{2D}}\} \tag{3.14b}$$

$$d_f = h_u - z_{\text{crest}} \tag{3.14c}$$

Where W is the weir width, A_{mh} the area of the node, C_o the orifice coefficient, C_{fw} the free weir coefficient, C_{sw} the submerged weir coefficient. Those weir and orifice coefficients could be obtained from physical experiment, like those presented by Rubinato et al. (2017).

The signed volumetric flow Q_e is positive when entering the surface model and negative when entering the drainage network. This process is shown in (3.15):

$$Q_e = Q \frac{h_{\text{mh}} - h_{\text{2D}}}{|h_{\text{mh}} - h_{\text{2D}}|} \tag{3.15}$$

3.2.3 Implementation

The implementation is done in several layers:

- The SWMM source code with additional API functions.
- A Cython (Behnel et al., 2011) wrapper for C functions that apply to network objects.
- A Ctypes (Kloss, 2008) wrapper for general SWMM functions.
- A set of Cython functions that resolve the surface–drainage coupling.
- A Python class that represents the general drainage model interface for interactions with Itzï.
- The general Itzï simulation manager, that manage the time-stepping synchronisation.

3.2.3.1 Modification of C code

The original SWMM code could be compiled as a shared library. It does export some functions to run simulation or write results, but none for changing simulation data during run time. It requires modifications that have been influenced by the work of Shrestha et al. (2012). Those are similar to the one proposed later by Leandro and Martins (2016). For example, to be able to set a new inflow at a node, a *DLLinflow* value has been added to the SWMM *Node* objects, which could be set externally and add to the SWMM *Inflow* existing variable. An exported function allows modification of this *DLLinflow* from outside (see Listing 3.1).

Similarly, and in addition to the SWMM internal data structures for nodes and links, two other data structures dedicated to the export of those objects values have been created. Listings 3.2 and 3.3 present an example of the data struture and function for the export of link values.

```
1  int DLLEXPORT   swmm_addNodeInflow(char* id, double inflow)
2  {
3      int index = -1;
4      if ( IsOpenFlag )
5      {
6          index = project_findObject(NODE, id);
7          if ( index < 0 )
8              return ERR_NAME;
9          Node[index].dllInflow += inflow;
10         return ERR_NONE;
11     }
12     return ERR_NOT_OPEN;
13 }
```

Listing 3.1: Additional C function to add an external inflow to a SWMM node (Shrestha et al., 2012).

3.2.3.2 Python wrapper

The Python wrapper has various functionalities. First, new Python *Exception* classes have been written to spot errors more easily. Especially, a Python *Exception* class has been created to map C return codes generated by SWMM, as C does not support exceptions handling.

```
typedef struct
{
    double flow;
    double depth;
    double velocity;
    double volume;
    int type;          // link type code
    double offset1;    // ht. above start node invert (ft)
    double offset2;    // ht. above end node invert (ft)
    double yFull;      // depth when full (ft)
    double froude;     // Froude number
} linkData;
```

Listing 3.2: The C structure dedicated to store links data for export from SWMM. This code is inserted in SWMM *objects.h*.

```
int DLLEXPORT   swmm_getLinkData(int index, linkData* data)
{
    if ( IsOpenFlag )
    {
        data->flow = Link[index].newFlow * Link[index].direction;
        data->depth = Link[index].newDepth;
        data->volume = Link[index].newVolume;
        data->velocity = link_getVelocity(index, Link[index].newFlow, Link[index].newDepth)
                         * Link[index].direction;
        data->offset1 = Link[index].offset1;
        data->offset2 = Link[index].offset2;
        data->yFull = Link[index].xsect.yFull;
        data->froude = Link[index].froude;
        data->type = Link[index].type;
        return ERR_NONE;
    }
    return ERR_NOT_OPEN;
}
```

Listing 3.3: The C function that populates a given linkData structure (see Listing 3.2) from the values of the internal Link SWMM structure.

Second, a SWMM input file parser has been created. It is used mainly to retrieve coordinates values from the input file, as those values are discarded by the SWMM engine and therefore not accessible with the C API. The *SwmmInputParser* class has been created to that end.

Finally, a *Swmm5* Python class as been written using ctypes, a Python package which allows calls to C functions from a Python software (Kloss, 2008). The developed python wrapper allows the following:

- Open, close, start and end a SWMM simulation.
- Advance a SWMM by one step.

On the Python side, the nodes and links data are stored as one-dimensional, structured NumPy arrays (Van Der Walt et al., 2011); the fields are equivalents to the exported C fields (see for example Listing 3.2). A class named *SwmmNetwork* is in charge of creating and manipulating those two arrays, and updating them with values from the C API. The update of those NumPy arrays is done through a Cython interface (Behnel et al., 2011) that allows fast loops among the SWMM objects. Two classes, *SwmmLink* and *SwmmNode*, are used as an interface to *SwmmNetwork* to retrieve values from a single element. The first version of Itzï that includes the drainage model is the 17.7. The results presented in this document are obtained with the version 18.2.

3.2.3.3 Drainage simulation reporting

Itzï exports the drainage simulation results as a GRASS vector time-series. This simplifies the visualisation and interpretation of results, especially when dealing with large networks. Each map is linked to two database (DB) tables. The first one stores the node values, and the second one the links values. The values stored in for nodes and links are shown in Tables A.1 and A.2, respectively. The exported vector maps contain instantaneous values for the considered time-step.

3.2.4 Validation

The coupled model is tested with the Environmental Agency test case number 8b, described by (Néelz and Pender, 2013). It represents a neighbourhood of Glasgow, UK of 966 × 402 m. It is similar to the test number 8a presented in Section 3.1.3.2. This synthetic case is designed to simulate the overflow of a drainage network in a urban environment.

3.2.4.1 Input values

The Digital Terrain Model (DTM) is obtained by LiDAR and have an original resolution of 0.5 m. It is resampled to 2 m by statistical mean. The buildings are incorporated in the DTM from a vector map. The resulting DEM and the position of manhole and control points is represented in Figure 3.8. As in the test 8a, the Manning's n is set to $0.02\,\mathrm{s\,m^{-1/3}}$ and $0.05\,\mathrm{s\,m^{-1/3}}$ for the road and the remaining of the area, respectively.

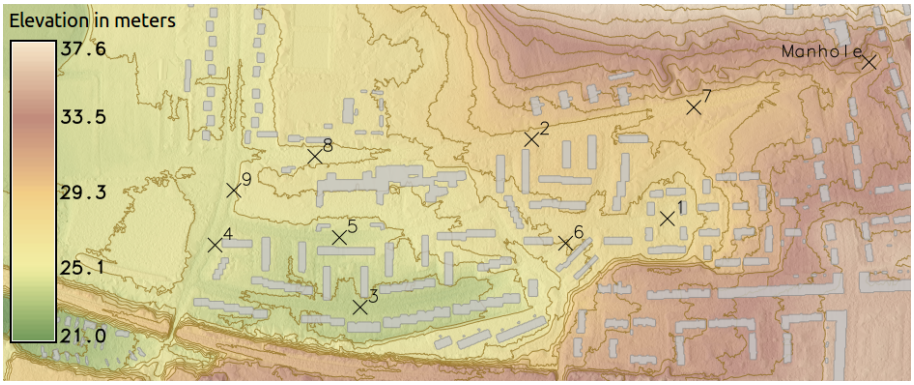

Figure 3.8: DEM of the study area, position of manhole and control points.

The fictitious drainage network is made of seven junctions and one outfall, all in the same branch. All pipes are circulars with a diameter of 1.4 m. An inflow is set in the most upstream junction of the pipe network. The hydrograph of this inflow is shown in 3.9. Only the second manhole is allowed to overflow into the domain, at the position showed in Figure 3.8.

Here, *Itzï* is compared with four other coupled models, that are taken as a reference:

- Infoworks ICM and Mike are popular commercial softwares.
- UIM (A. S. Chen et al., 2007) is based on simplified diffusive wave equations.
- xpstorm uses SWMM as the network model.

In particular, Itzï will be conmpared tu xpstorm because they both use SWMM as the drainage model. They are therefore expected to give similar results, especially for the manhole outflow. Figure 3.10 shows the outflow from the drainage network calculated by those modelling packages.

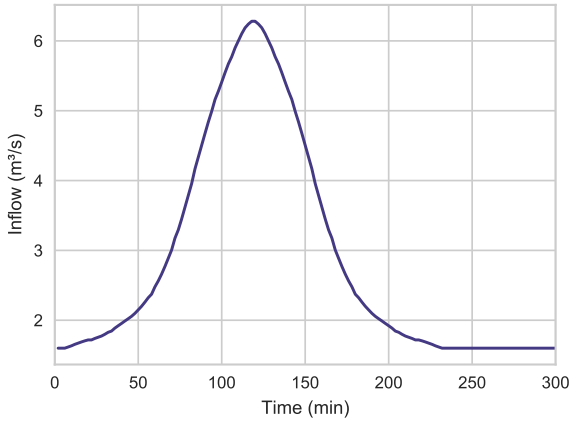

Figure 3.9: Upstream inflow of the pipe network.

The results obtained by Itzï in different configurations are presented in Figure 3.11. Some instabilities occur in the flow exchange at the manhole when the orifice coefficient C_o is set to 1. They are due to oscillations that happen when the water head in the surface model is close to the head in the drainage node. In that specific test case, this condition occurs at the beginning and at the end of the overflowing event. Those oscillations are controlled in Itzï by preventing the sudden inversion of flow from/to the surface, as shown in (3.16):

$$Q_e^{\Delta t_{1D}+t} = \begin{cases} 0, & \text{if } (Q_e^{\Delta t_{1D}} < 0) \wedge (Q_e^{\Delta t_{1D}+t} > 0) \\ 0, & \text{if } (Q_e^{\Delta t_{1D}} > 0) \wedge (Q_e^{\Delta t_{1D}+t} < 0) \\ Q_e^{\Delta t_{1D}+t}, & \text{otherwise} \end{cases} \tag{3.16}$$

Additionally, to prevent negative water depth in the overland flow model, Itzï limits the inflow into the drainage network according to volume in the coupled cell. This process is shown in (3.17):

$$Q_{\text{link}} = \begin{cases} \max\{-\dfrac{d_{2d} A_{\text{cell}}}{\Delta t_{1D}}, Q_e\}, & \text{if } Q_e < 0 \\ Q_e, & \text{if } Q_e \geq 0 \end{cases} \tag{3.17}$$

where Q_e is the volumetric exchange flow being positive when leaving the drainage, d_{2d} the water depth in the surface cell, A_{cell} the raster cell area and Δt_{1D} the time-step of the drainage model.

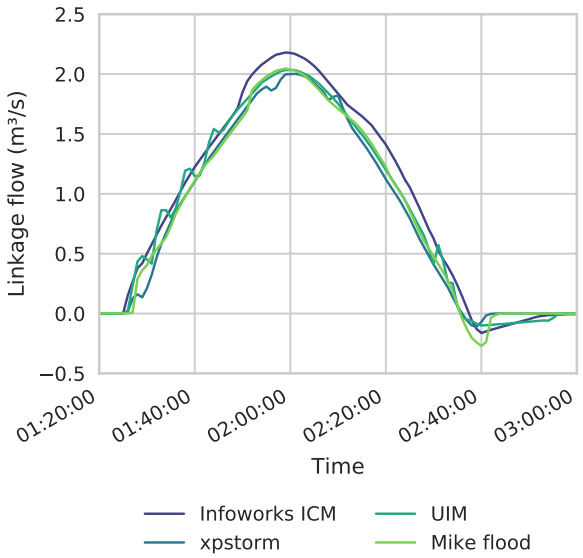

Figure 3.10: Linkage flows at the manhole obtained by commercials and academic models. Adapted from Néelz and Pender (2013).

For further stability, Martins et al. (2017) propose an additional flow limiter when the flow exits the drainage model. This flow limiter has an high impact on the calculated flow rate, and is used to mitigate limited observed instabilities. Therefore, Itzï does not implement that additional flow limiter proposed by Martins et al. (2017). However, Itzï is set to use by default the orifice and weirs coefficients obtained from physical experiments by Rubinato et al. (2017). Those coefficients are presented in Table 3.2. When using those values, the solution become much more stable, albeit with a smaller flow rate than the reference model (see Figure 3.11). Figure 3.11 shows the impact of using either no orifice coefficient ($C_o = 1$), the experimental orifice coefficient (Rubinato et al., 2017), and a node outflow limiter (Martins et al., 2017). This plot demonstrates that without an orifice coefficient or a node outflow limiter, Itzï manages to maintain an acceptable stability that compares very well with the commercial model xpstorm. Indeed, when compared to xpstorm, the node coupling flow obtained by Itzï with the above-mentioned settings results in a Nash-Sutcliffe Efficiency (NSE) above 0.99 and a ratio of the root mean square error to the standard deviation of reference data (RSR) inferior to 0.1. Those statistics are considered to be 'very good'

according to the criteria set by Moriasi et al. (2007). When using the orifice coefficient recommended by Rubinato et al. (2017), the computed outflow is lower than xpstorm and the other reference models, but also more stable. A similar result is obtained when using the outflow limiter proposed by Martins et al. (2017).

Table 3.2: Orifice and weirs coefficients used by Itzï and adapted from Rubinato et al. (2017).

Coefficient	Value
C_{fw}	0.54
C_{sw}	0.056
C_o	0.167

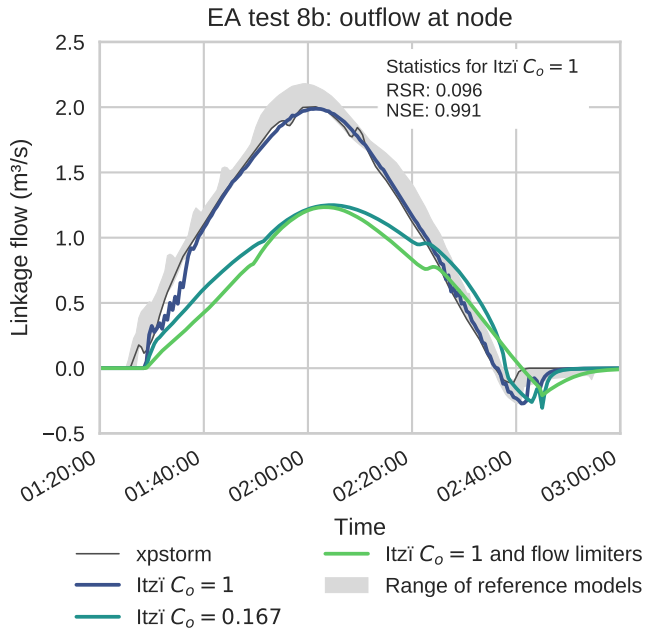

Figure 3.11: Computed outflows at the manhole in the EA test 8b, showing the impact of the orifice coefficient C_o from Rubinato et al. (2017) and the flow limiters proposed by Martins et al. (2017). xpstorm and range of reference models values from Néelz and Pender (2013).

Figure 3.12 shows the evolution in time of the water depth at two control points. Although the flood wave from Itzï arrives later than the one obtained with xpstorm, the RSR and NSE statistics are still considered 'very good' according to the classification made by Moriasi et al. (2007). When setting the orifice coefficient to a value in line with those proposed by Rubinato et al. (2017) (see Table 3.2), the flood wave calculated by Itzï arrives 10 to 20 min later than xpstorm. At Point 1, the final water depth is equal to the one obtained with a coefficient of 1. At Point 3 however, the final water depth is lower, due to the lower volume of water coming out of the drainage. Moreover, it should be noted that in this test 8b, the compared models used different DEM interpolation techniques. This resulted in differences in water depth obtained by the models at a given point (Néelz and Pender, 2013).

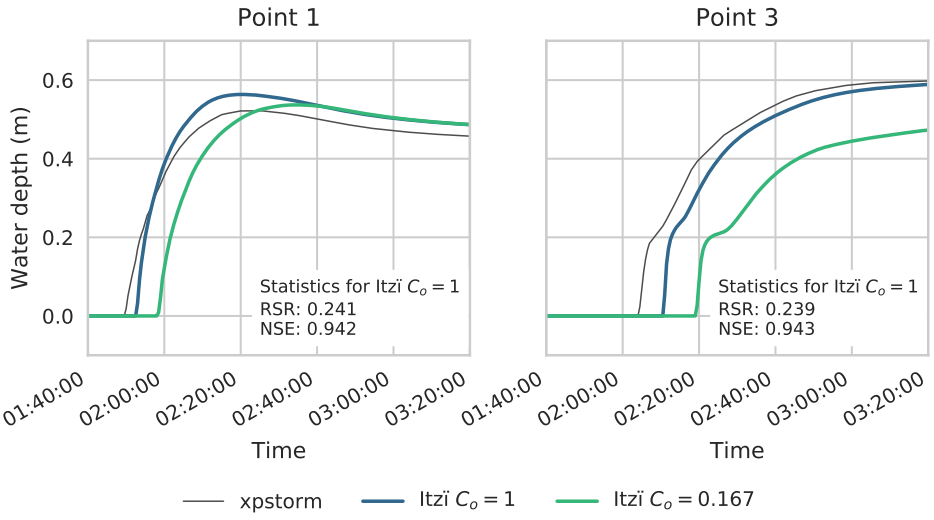

Figure 3.12: Water depth at control points. xpstorm values from Néelz and Pender (2013).

4 Case studies

4.1 Reproduction of the June 2007 floods in Hull, UK

This Section has been published as:

> Courty, L. G., M. Á. Rico-Ramirez and A. Pedrozo-Acuña (2018). 'The Significance of the Spatial Variability of Rainfall on the Numerical Simulation of Urban Floods'. In: *Water* 10.2, p. 207. DOI: 10.3390/W10020207. URL: http://www.mdpi.com/264172.

4.1.1 Introduction

With the advent of computational methods and computer processing power, the ability to tackle urban floods at a catchment level is clearly emerging, making it possible to apply an integrated approach to modelling rainfall-runoff processes along with surface flows (Courty et al., 2017; Yu and Coulthard, 2015). Moreover, the availability of new data sources with higher quality and spatio-temporal resolution (e.g. rainfall data estimated by radars and terrain data derived from LiDAR) enables a more detailed description of hydrological processes that occur in the real world, paving the road towards a better numerical discretisation of the processes involved in urban floods.

On the other hand, the documented growth in the number of floods and urban population due to climate change (Hirabayashi et al., 2013), clearly indicate the importance of an improved understanding on how flood waters interact with the urban environment both in space and time. Indeed, the development of a reliable approach to adequately describe

urban flood processes has been recognised as a challenging task (Vojinović and Abbott, 2012).

Recent advances in urban flood modelling recognise the importance of 2D modelling algorithms to adequately reproduce urban floods (N. M. Hunter et al., 2008). However, it should be borne in mind that model performance also depends on the quality of data used to construct a numerical representation of the catchment and rainfall. This information includes soil characteristics, land use, topography and forcing conditions, all of which play an important role in the generation of an urban flood. (Di Baldassarre, 2012; Zevenbergen et al., 2010) In reality, this data varies in space and time, and its representation at an adequate spatio-temporal resolution is necessary for an accurate performance of the numerical tool. However, datasets are rarely homogeneous in space and time, which leaves the door open to the exploration of an adequate level of complexity and detail for this purpose.

Among the main factors identified to adequately reproduce urban floods, the uncertainty of rainfall distribution in time and space is one of the main sources of error (Cristiano et al., 2017). It is well known that a good knowledge of precipitation at appropriate spatial and temporal scales enhances modelling of rainfall-runoff processes in urban catchments (Arnaud et al., 2002; Bruni et al., 2015; Cristiano et al., 2017; Gires et al., 2012; Rico-Ramirez et al., 2015; Segond et al., 2007). Accurate estimations of precipitation in urban areas require a dense rain gauge network combined with an effective analysis method. However, rain gauge networks are generally too sparse spatially to provide such detailed information (Seo, 1998). On the other hand, information acquired with weather satellites enable a better spatial description of rainfall fields, but also lack a proper spatial resolution for urban applications with grids of 10 km or coarser (Nesbitt and Anders, 2009; J. A. Smith et al., 2007). Furthermore, weather radar measurements are inherently uncertain to some degree, as the relationship between reflectivity and actual rainfall on the ground requires the derivation of empirical coefficients (J. A. Smith and Krajewski, 1993). An alternative way of making use of this data is to blend rain gauge and weather radar data (Ercan and Goodall, 2013; Goudenhoofdt and Delobbe, 2009; Velasco-Forero et al., 2009).

In the literature, when modelling urban floods, it has been largely recognised that the spatial variability of rainfall is a source of uncertainty that affects model performance. However, most of the publications

aimed at the investigation of this topic have considered theoretical scenarios, with little reference to case studies of actual events (Cristiano et al., 2017). Therefore, more research is required that incorporates case studies from the real-world, and that investigate how the spatial variability of rainfall affects flood predictions in urban environments. This could be done by studying multiple events and locations that variate parameters like catchment size, percentage of urbanization, topography and quality of available rainfall data. To that end, we propose here a step in that direction by studying the impact of rainfall variability on the reproduction of a real-world urban flood event.

The case study corresponds to the urban flood registered in the United Kingdom on June 25th 2007, when the city of Kingston upon Hull (herein later referred to as Hull), East Yorkshire, suffered heavy flooding that affected 8600 homes and 1300 businesses (Coulthard and Frostick, 2010). Although the numerical reproduction of this event has been reported in Yu and Coulthard (2015) or Courty et al. (2017), the integration of spatially variable rainfall has not been discussed or attempted. Both numerical approaches resolve the inertial equation proposed by Bates et al. (2010), incorporating the Green–Ampt formula to simulate the infiltration process, differing only in the way the adaptive time-step is implemented. Notably, in both studies, rainfall was considered using hourly measurements of only one rain-gauge located at the University of Hull. Therefore, the precipitation was assumed to be spatially uniform within the catchment.

The purpose of this study is to investigate how a better definition of the spatial variability of rainfall improves the numerical reproduction of the severe floods registered in Hull, UK in 2007. Flood maps derived from the use of a uniform rainfall field against those resulting from a merged product from weather radar and rain gauge data will be compared and discussed. Focus will be given to the western part of the city of Hull, which was the most affected according to Coulthard and Frostick (2010).

This paper is organised as follows: Section 4.1.2 introduces the flood inundation model used to replicate this event as well as the forcing data required to run the model; Section 4.1.3 presents the calibration process and the results; Section 4.1.4 discusses the outcomes in light of similar studies and summarises the main conclusions derived from this investigation.

4.1.2 Material and methods

4.1.2.1 Computer model

In this study we employ the version 17.8 of Itzï (See Section 3.1 for a detailed description). The modelling parameters shown in Table 4.1 are the same for each simulation. All the boundaries of the computational domain are closed.

Table 4.1: Modelling parameters

Parameter	Value
α	0.7
$\Delta t_{\text{2D max}}$ (s)	2.0
θ	0.7

4.1.2.2 Input data

Study area

Kingston upon Hull, abbreviated as Hull, is a British city located on the northern shore of the Humber estuary, in the East Riding of Yorkshire, England (see location map in Figure 4.1). The city proper hosts 260 200 inhabitants, while the population of the larger urban zone is 573 300. Hull possesses a oceanic climate, with an annual precipitation of 674 mm and 15 days a year of heavy rainfall (Klein Tank et al., 2002).

Elevation

For this study we use a DEM obtained from aerial LiDAR. Its spatial resolution is 5 m. It can be see in Figure 4.2 that the study area could be divided in two zones. The western part is a hillside while the eastern part is mostly flat with some areas below the mean sea level. The constructed area is concentrated in the flat eastern part.

Observed flood extents

After the event, the Hull City Council (HCC) and the EA evaluated the extension of the affected areas. While the EA used aerial photography

to map the flooded areas, the HCC carried out a poll among the residents (Coulthard and Frostick, 2010). The areas identified by each administration are represented in Figure 4.3. It could be noted that the two zones classified by the two administrations shows significant differences highlighted in Table 4.2. Notably, less than half of the individual observations could be validated by the other. Furthermore, due to the limitations of the collection methods, it is possible that the identification of the flooded areas is partial and that some actually affected areas might not be represented (Coulthard and Frostick, 2010).

Friction

The Manning's n friction map is created using the Global Land Cover (GLC30) map from the National Geomatics Center of China (J. Chen et al., 2014). Figure 4.4 shows the map of the repartition of the land cover classes over the study area. Typical values of n from the literature are assigned for each cell according to its class (Chow, 1959). Table 4.3 shows the relation between the land cover classes and the Manning's n values proposed by Chow (1959).

Drainage

The drainage of the city of Hull is entirely pumped because of the topographic situation of the urban area (Coulthard and Frostick, 2010). The drainage of the study area was carried out by the combined action of the following pumping stations that worked continuously during the event (Coulthard and Frostick, 2010):

- West Hull pumping station (capacity $32\,m^3\,s^{-1}$), draining the whole study area plus a smaller part of the city north of it.
- Saltend Waste Water Treatment Work (outflow $22\,m^3\,s^{-1}$), treating most of Hull, including the study area.

Yu and Coulthard (2015) mention drainage capacity values for Hull of $70\,mm\,d^{-1}$ for the urban area and $15\,mm\,d^{-1}$ for the rural areas. Applying $70\,mm\,d^{-1}$ of drainage capacity to the urbanized part of the study area (See Figure 4.4) represents an average flow of $30.64\,m^3\,s^{-1}$. This value is coherent with the installed pumping capacity described above. Therefore, we created a drainage capacity map using the values from Yu and Coulthard (2015) on the urban and non-urban areas defined by the GLC30 map (See Figure 4.4). The artificial surfaces have been assigned a value of $2.917\,mm\,h^{-1}$ and the remaining areas $0.625\,mm\,h^{-1}$.

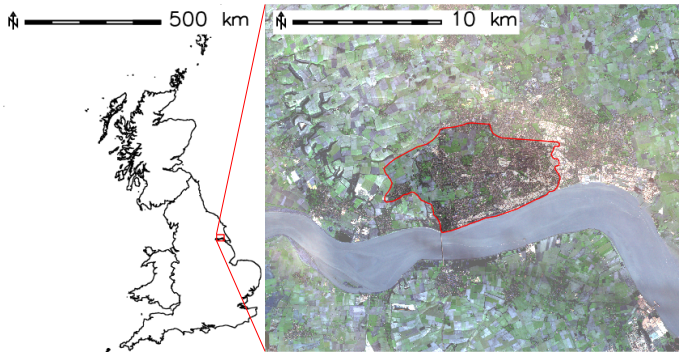

Figure 4.1: Location of the Hull study area within Great Britain (satellite imagery Copernicus Sentinel 2016). (Courty et al., 2017)

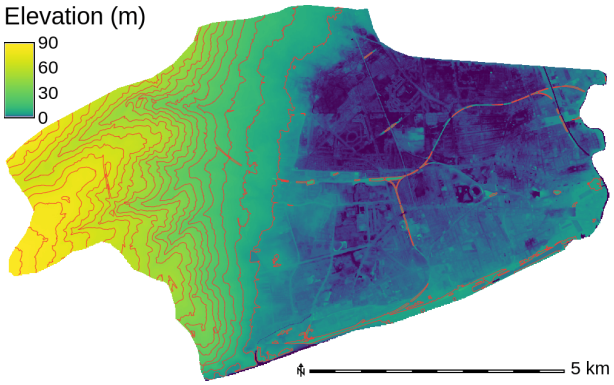

Figure 4.2: Digital Elevation Model of the study area. Contour lines are every 5 m.

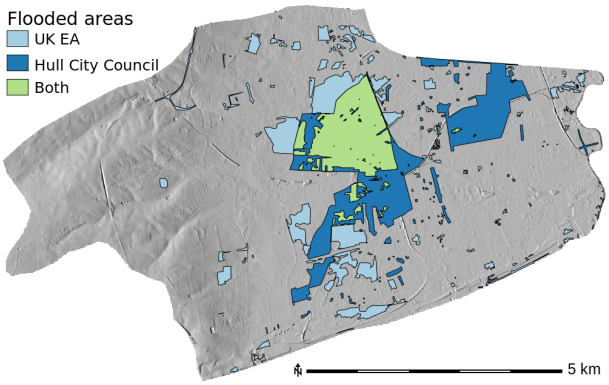

Figure 4.3: Identified flooded areas. Light blue: EA only. Dark blue: HCC only. Green: Intersection of both administrations.

Table 4.2: Comparison of identified flood extents

Collecting entity	Area (km^2)
Environment Agency	5.16
Hull City Council	6.18
Intersection of both	2.33

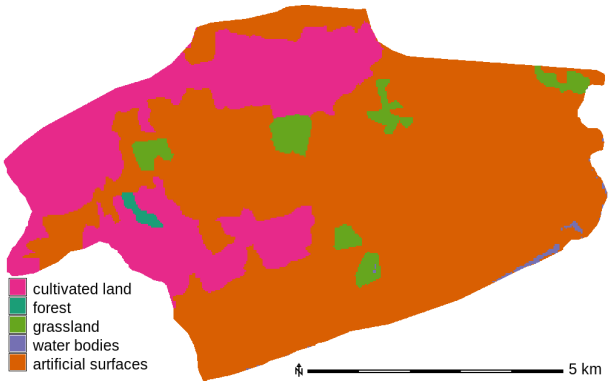

Figure 4.4: Land cover classes from Global Land Cover in the study area

Table 4.3: Relation between land cover classes and Manning's n values.

GLC30 class	Category from Chow (1959)	Manning's n ($s\,m^{-1/3}$)
Cultivated land	Mature field crops	0.040
Forest	Cleared land with tree stumps, heavy growth of sprouts	0.060
Grassland	Pasture with short grass	0.030
Water bodies	Natural stream: clean, straight, full stage, no rifts or deep pool	0.030
Artificial surfaces	Gunite, good section	0.019

Infiltration

Coulthard and Frostick (2010) estimate that the soil was saturated due to the important rainfall prior to the studied event. Therefore, we consider that the infiltration could range from naught—where no infiltration at all happens—to a value depending on the hydraulic conductivity of the soil. We estimated the possible hydraulic conductivity over the study area with the help of the global soil database SoilGrids250m (Hengl et al., 2017). First, we calculate the average clay and sand values in the top 60 cm of soil. Then we use the resulting maps to classify the soil according to textures definitions from the United States Department of Agriculture (USDA). Finally we relate the texture classes with typical values obtained from experiments (Rawls et al., 1983). Table 4.4 displays the values obtained by this methodology. The average hydraulic conductivity estimated in the study area is $3.57\,\mathrm{mm\,h^{-1}}$.

We acknowledge the uncertainty of the method used to estimate the conductivity, especially in a urban environment, and use uniform values of infiltration for model calibration. We consider the infiltration to be equal to the hydraulic conductivity, which is consistent with the Green–Ampt equation when used in saturated soils. Therefore, the infiltration values we use for the model calibration are 0 to $5\,\mathrm{mm\,h^{-1}}$ with a $1\,\mathrm{mm\,h^{-1}}$ step.

Table 4.4: Distribution of estimated hydraulic conductivity above the study area.

Hydraulic conductivity ($\mathrm{mm\,h^{-1}}$)	Surface (ha)	Surface (%)
1.00	18.88	0.30
1.50	654.5	12.0
3.50	4507.5	82.3
10.9	295.6	5.40

Precipitation

For the Precipitation we compare two sources of information. The first one is the measurement from an uncalibrated rain gauge at the University of Hull (Yu and Coulthard, 2015). Its temporal resolution is of 1 h and it is considered uniform in space. The second one is a time-series of

raster maps reconstructed using various rain gauges and a meteorological radar. Although radar rainfall provides spatial rainfall information, it fails to estimate the correct intensity, partly because it may be affected by different sources of errors. On the other hand, rain gauges can measure the point rainfall intensities more accurately, but are unable to provide information on the spatial rainfall distribution. Merging the two sources of rainfall data is recognised to improve the estimates (Goudenhoofdt and Delobbe, 2009; Haberlandt, 2007; Jewell and Gaussiat, 2015; Schuurmans et al., 2007; Wilson, 1970). The selected radar-gauge merging method is Kriging with External Drift (KED) (Chiles and Delfiner, 2012; Cressie, 2015). KED assumes the mean of the process (drift) as a linear function of external covariates. In this case, the only considered covariate is the radar rainfall.

For this event, we use the Weather radar rainfall composite product from the UK Met Office at 1 km and 5 min spatial and temporal resolutions (Harrison et al., 2009) and a series of rain gauges from the EA to create the raster time-series using KED. The radar rainfall product has been quality-controlled by the UK Met Office and it has been corrected for well-known sources of error in radar rainfall (Met Office, 2003). Note that the urban area was mainly covered by the Hameldon Hill radar located more than 100km towards the West of the urban area. Figure 4.5 shows the map of accumulated precipitation together with the locations of the weather radar and rain gauges. Due to the distance of the radar from Hull, the actual radar rainfall spatial resolution above the study area is around 5 km. Furthermore, the radar rainfall had gaps in data during this event and therefore the missing time periods were interpolated using a nowcasting model (Liguori and Rico-Ramirez, 2014). Unfortunately some of the missing periods occurred during the time of heavy precipitation falling on the study area. The spatial resolution of the resulting rainfall field is of 1 km. The radar rainfall scans were accumulated to produce a temporal resolution of 1 h, similar to the uniform rainfall. Figure 4.7 shows the evolution in time of the rainfall field generated by KED. Note that some time steps shown in Figure 4.7 show a KED spatial rainfall resolution of 1 km due to the fact that the radar-gauge KED merging was performed at 1 km resolution and also because the nowcasting model to interpolate the missing time periods also runs at 1 km.

The mean hyetographs of each rainfall, average above the urban area, are compared in Figure 4.6. The peak intensity of the KED rainfall is lower than the uniform rainfall, but at lower intensity, the KED rainfall shows

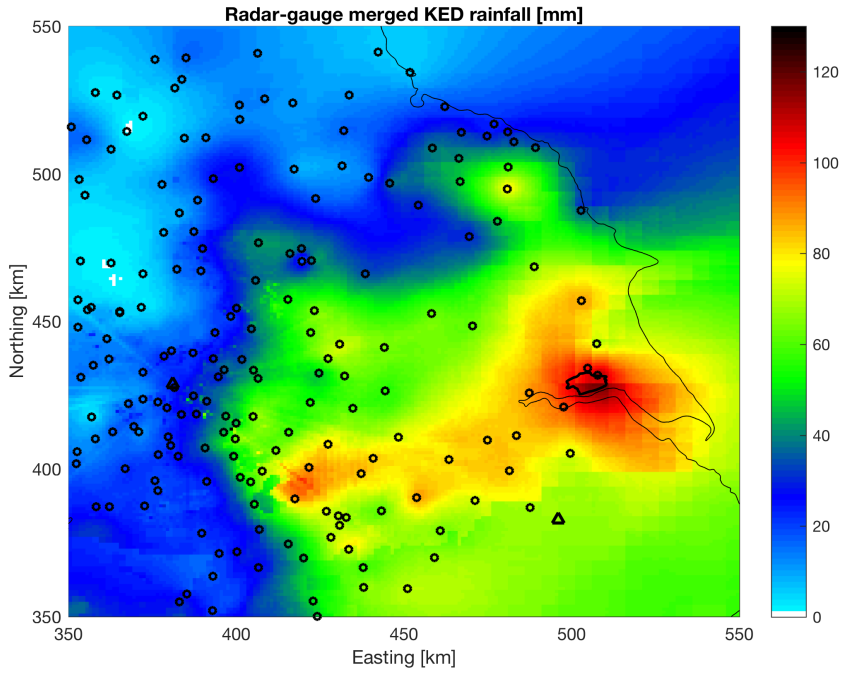

Figure 4.5: Accumulated rainfall obtained from Kriging with External Drift on 25 June 2007. Circles represent the rain gauges used. Triangles are the weather radars. The study site is represented by a black polygon. Please note that during this event, only Hameldon Hill radar (located at the west of the region) was operating.

higher values. On the same figure is represented the range of intensity values that are present in the raster rainfall field obtained by KED. This allow for a better understanding of the spatial variability of the rainfall during this event. The spatial variability of the KED rainfall is higher when the intensity is higher. The precipitated volumes during the event are 6.1 hm^3 and 5.9 hm^3 for the uniform rainfall and the KED rainfall, respectively.

4.1.3 Results

We first calibrate the model with the uniform rainfall using the infiltration as a calibration value. Secondly, we run an additional simulation using

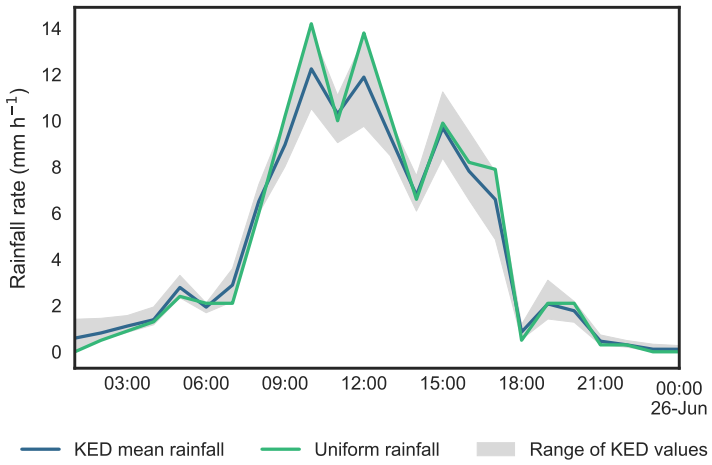

Figure 4.6: Hyetographs of the two considered rainfalls above the study area on 25 June 2007.

the calibrated values and the KED rainfall. We then compare the results obtained with the KED rainfall to those obtained with the uniform rainfall. To do so, we subject the results to two types of analysis; a qualitative one and a quantitative one.

4.1.3.1 Model calibration

Since this case is not sensitive to friction (Yu and Coulthard, 2015) we select only the infiltration as a calibration value. As mentioned in Section 4.1.2.2 we use the uniform infiltration values of 0, 1, 2, 3, 4 and 5 mm h^{-1}. For this process of calibration, we use the uniform rainfall. We calibrate the model using the identified flood extent as references. We have two maps of flood extent (see 4.1.2.2). We use as reference those two maps plus a union of those two extents.

In order to compare the computed flooded areas to the observed ones, we classify each cell as flooded or dry by applying a water depth threshold on the computed water depth. There is no definite literature on the value of this threshold and it is mostly arbitrary (Wilks, 2011). Therefore, we use a series of 31 values from 0.5 to 35 cm distributed with a 1 cm step. Logically, the generated binary maps shows a larger extent of inundation when the threshold is lower, and a smaller extent with a higher

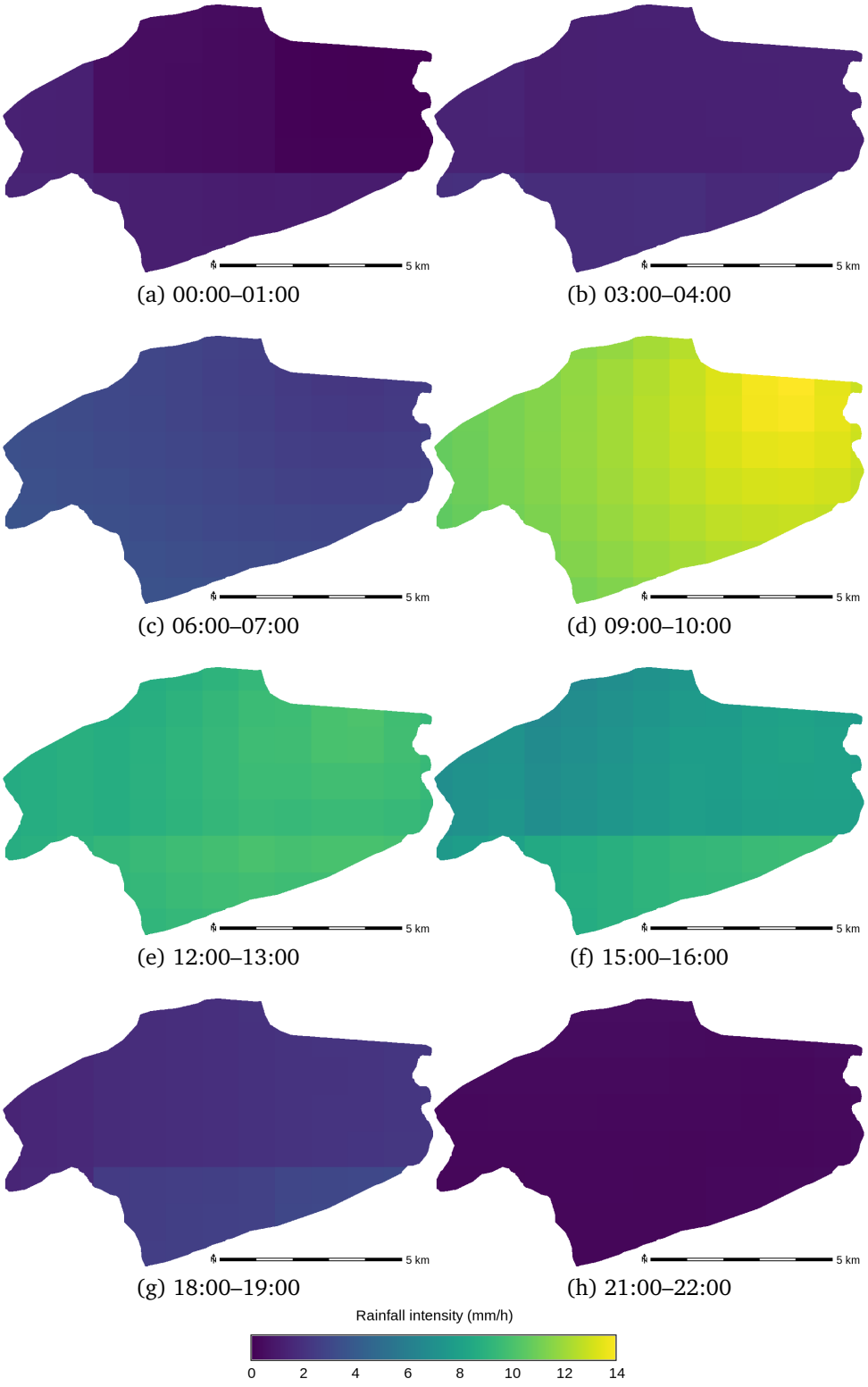

(a) 00:00–01:00 (b) 03:00–04:00

(c) 06:00–07:00 (d) 09:00–10:00

(e) 12:00–13:00 (f) 15:00–16:00

(g) 18:00–19:00 (h) 21:00–22:00

Figure 4.7: Evolution of rainfall intensity above the study area obtained with Kriging with External Drift. Event of the 25 June 2007.

threshold. The first step to compare those generated maps to the observed extent maps is to classify the results in a contingency table (see Table 4.5). This contingency table is then used to calculate the Critical Success Index (CSI) (Wilks, 2011), a skill evaluation score commonly used in hydrology (e.g. Cook and Merwade, 2009; Horritt and Bates, 2002). This score is calculated using $\text{CSI} = \frac{\text{hits}}{\text{hits} + \text{misses} + \text{false alarms}}$. The combination of entry data that obtains the highest CSI will be used as a reference simulation to compare the two rainfall data.

Table 4.5: Contingency table used to calculate the Critical Success Index.

		Observed	
		Flooded	Not flooded
Computed	Flooded	hits	false alarms
	Not flooded	misses	correct negatives

The computed values of CSI obtained of the 6 simulations is shown in Figure 4.8. Each individual observed extent gives a lower value of CSI than the union of both extents. In that latter case, the highest value of CSI is obtained without any infiltration and at a water depth threshold of 20 cm. This highest CSI value is 0.36. Therefore, we retain the following calibration values:

- Union of observed flooded extents as the 'real-world' reference.
- No infiltration.
- Water depth threshold of 20 cm.

4.1.3.2 Qualitative analysis

During the event, the water accumulates in the lower part of the domain, which is also the most urbanised. Figure 4.9 compares the computed maxima water levels with the observed extents. It shows that the model is able to identify the main flooded area observed by the two collecting entities, at the centre of the domain. For the other inundated parts, the comparison is more difficult because of the discrepancies between the observations of the EA and the HCC.

Some differences in computed water level occurs between the simulation using the KED rainfall and the one using uniform rainfall. Those differences are not easily noticed on Figure 4.9. Figure 4.10 allows an

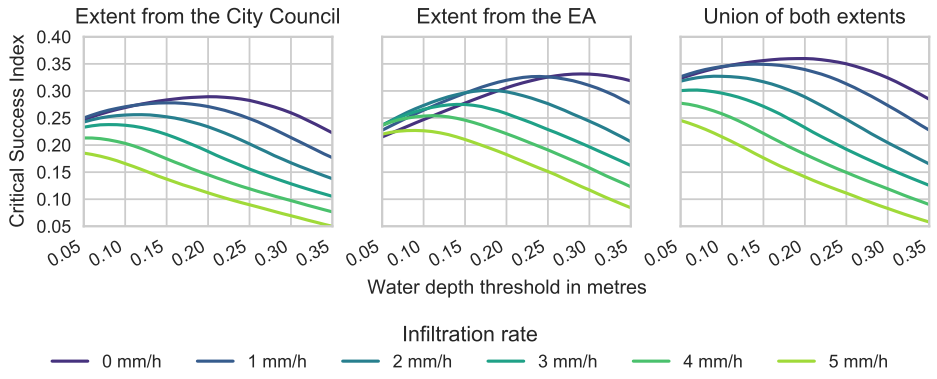

Figure 4.8: Values of Critical Success Index obtained during the calibration process. They are obtained with uniform rainfall and different infiltration values, water depth thresholds and observed extents.

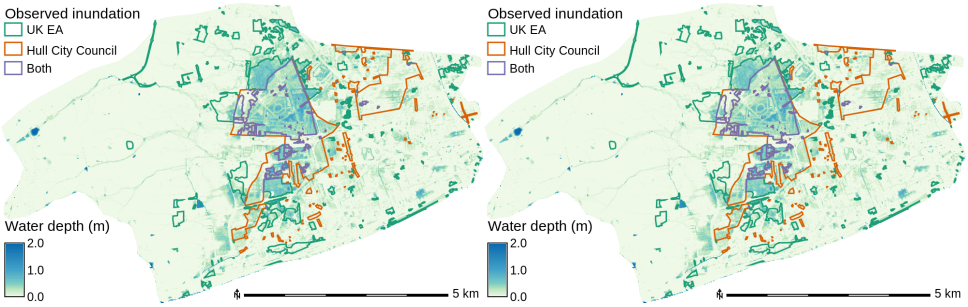

(a) Uniform rainfall (b) Kriging with External Drift

Figure 4.9: Comparison between observed extents and maxima computed water depths.

easier representation of those differences in maxima water depths. It could be noted that water levels obtained using the KED are consistently lower than those using the uniform rainfall. This could be related to the smaller precipitated volume of the KED rainfall (see Section 4.1.2.2). The discrepancies are mostly between 5 to 10 cm, and is larger going eastward. In more limited areas, the differences reach 15 cm. Those higher differences in the eastern part of the domain might be due to the inundation being mostly due to the overland flow coming from the upstream areas on the west, and not from the local precipitation. The observed difference might therefore be due to the flood wave not reaching that far east when the precipitated volume is lower.

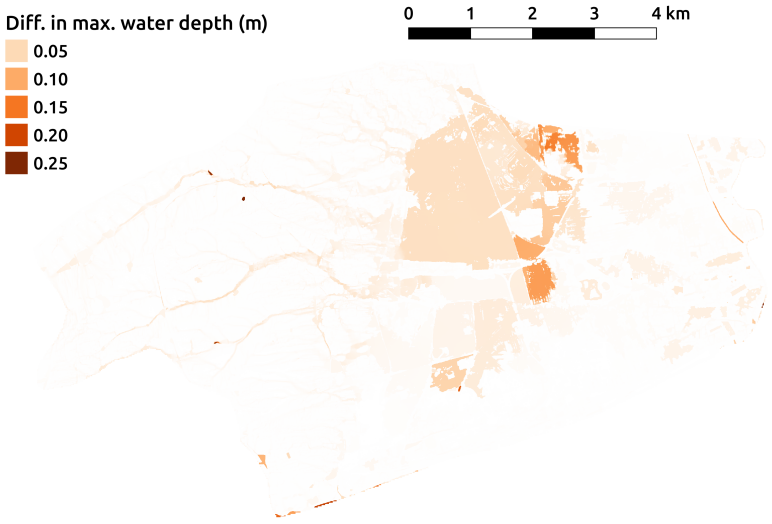

Figure 4.10: Differences in maxima water depths between the results using uniform rainfall and those using Kriging with External Drift. Here is shown the case without infiltration.

4.1.3.3 Quantitative analysis

In order to compare the results obtained with the uniform rainfall and those obtained with the KED, we calculate for each simulation result the CSI, total flooded area and percentage of the computational domain

which is flooded. Those calculations are first done with maxima water depths map, then we proceed to do a similar analysis with the evolution in time of those values along the simulation. For all those analysis we employ the values determined by the model calibration (see Section 4.1.3.1).

First, we compare the maxima water depth maps obtained by the two rainfalls. Table 4.6 shows the results of this analysis. The surface flooded is lower when using the KED rainfall. This is explained by the lower accumulated precipitated volume of the KED rainfall compared with the uniform rainfall (see Section 4.1.2.2). About the skill, the CSI obtained with each of the rainfall are quite weak, with values lower than 0.4. However, the uniform rainfall results in a CSI slightly higher than the KED, with 0.36 against 0.35.

Table 4.6: Comparison in maximum flooded areas between uniform and Kriging with External Drift rainfalls.

Rainfall	CSI	Flooded area (ha)	Surface flooded (percent)
Uniform	0.36	934.62	17.07
KED	0.35	861.06	15.73

Second, we examine the evolution in time of the flooded area, the flood volume and the CSI. Figure 4.11 shows the plots in time of those values obtained with the two different rainfalls. We can notice that the rate of change of all three values is logically affected by the intensity of the rainfalls (see Figure 4.6), with the steepest increase being between 07:00 and 17:00. The flooded volumes obtained with the two rainfalls reaches its highest value at the same time, 17:00. However, the flooded area continue to grow afterwards, with a peak occurring at 20:00. This is likely due to the spreading of the inundation continuing at smaller depths, resulting in a growing flooded area, even though the volume is getting smaller. Considering the CSI, the values obtained with the uniform rainfall are higher than those obtained with KED for most of the simulation. However, the difference is getting much smaller as the water level stabilize. With the uniform rainfall, the CSI peaks at 21:00 with a value of 0.445, while with the KED it peaks at 21:30 with a value of 0.439. At the end of the simulation, the CSI values for uniform and KED rainfall are 0.436 and 0.434, respectively. Furthermore, it is notable that the maximum CSI obtained during this exercise are higher than those obtained

with the maximum water level (See Table 4.6). We can explain that by the fact that the maxima water depths map includes the water channels that form in the more hilly west part of the basin (See Figure 4.9). This creates flooded cells in those area which are not reported as flooded by any of the two authorities, inducing a lower skill for both of the tested rainfalls. On the other hand, those channels dry out when the rain stops, which induces a higher CSI when calculating it using maps of instant water depth. This fact is reflected in the differences observed between the flooded areas calculated by snapshots water depths (816 ha) to the one obtained with the maxima water depths (935 ha, see Figure 4.6).

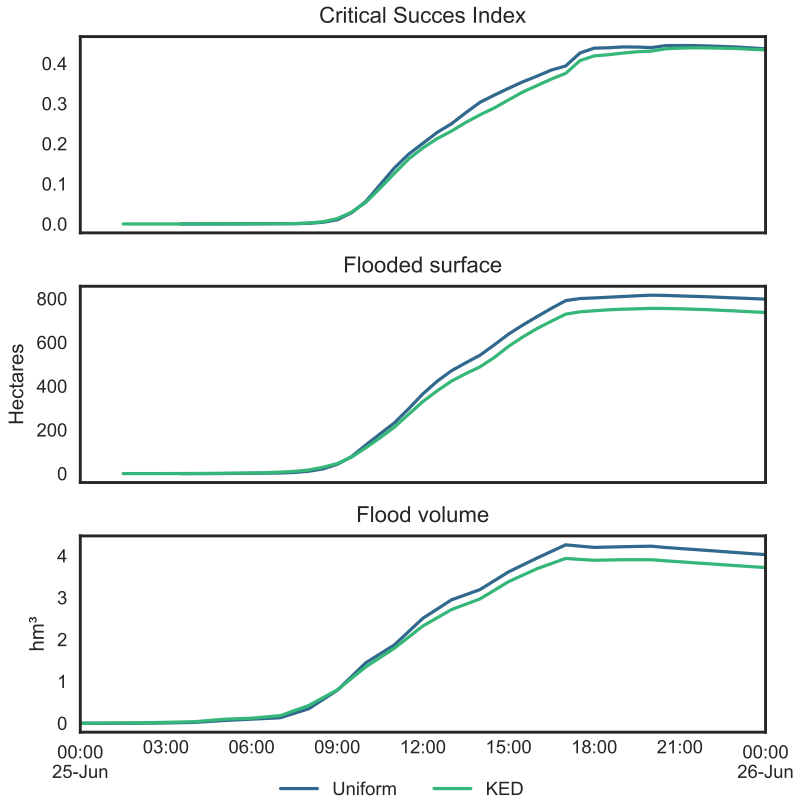

Figure 4.11: Evolution in time of the flood volume, flooded surface and Critical Success Index. The flooded surface and CSI are calculated for water depths above 20 cm.

4.1.4 Discussion and conclusions

In this paper we compared the computer simulation results obtained by the use of uniform and KED rainfall to observed inundation extents of the historical event of June 2007 in Hull, UK. Although the spatial variability of the KED rainfall is slight (see Figure 4.7), differences appear. For instance, the flooded area obtained with the KED rainfall is 8 % lower than the one obtained with the uniform rainfall (see Table 4.6). This is due to a lower precipitated volume and, in turn, a lower flooded volume when using the KED. However, those differences in flood volume and inundated areas do not reflect in the skill scores obtained by the two rainfalls when comparing the computed flood extents to the observations of actual affected zones. Indeed, the differences in CSI for those two rainfalls are not sufficient to be conclusive and should not be used to assert the superiority of one rainfall data against the other.

Two factors inherent to this specific event might influence those results. First, the observations of flooded zones are unlikely to accurately identify the affected areas (see Section 4.1.2.2). This uncertainty in the observations reduces the reliability of the calibration and evaluation processes. Second, the available radar data for this event come from an equipment rather far from the study area. This results in a practical spatial resolution of around 5 km. Furthermore, there were missing time periods in the radar data that needed to be filled using nowcasting interpolation before preforming the KED radar-gauge merging.

Unfortunately, uncertain or scarce observations are common during extreme flood events (e.g. Pedrozo-Acuña et al., 2014). Maps of observed flooding are especially difficult to obtain in urban areas due to the short time scale of their occurrence (usually a few hours). Few urban areas are instrumented, and remote-sensing techniques might be of limited use (Di Baldassarre, 2012). In addition to the relatively low revisit time of spacecrafts carrying high-resolution instruments, some technologies like multi-spectral imagery are seldom usable because of the cloud cover during or immediately after the precipitation event. In that sense, in spite of the limitations of the available data, the present case study can be considered data-rich because it includes both non-uniform rainfall data and observations of the affected areas.

Therefore, this study is a step forward in the direction of having a better understanding of the impact of the spatial variation of rainfall on the flood modelling of historical events. It shows that even with limited and

uncertain data, the incorporation of the spatial variability of rainfall does have an impact in the numerical results. We can mention that should another flooding event occurs in the same area, the definition of the rainfall data might improve due to the inclusion of the data of the Ingham radar, on the south of the study area (see Figure 4.5), that in turn might improve the reproduction of the inundation. Each event is different, and the relative size of the precipitation compared to the study area is to be considered. In urban areas of limited extent like Hull, more localized events like convective precipitations might require even more the consideration of the spatial component of rainfall. More similar studies should be carried out in the future that will tackle the subject with other type of events and study areas, including different type of meteorological events, topography and land use.

4.2 Reproduction of the July-August 2015 flood in Kolkata, India

Kolkata is a city located in the Ganga delta, in the Indian state of West Bengal. During monsoon it regularly suffers from floods. The studied area is located on the left bank of the Hoogly river, a distributary of the Ganga river. Figure 4.12 shows the location of the study area relative to the Republic of India and the state of West Bengal. In this section I'll present the study of the reproduction of the event that occurred from the 31 July to 1 August 2015. Most of the data are kindly provided by Dr. Dhrubajyoti Sen from the Indian Institute of Technology at Kharagpur.

4.2.1 Entry data

4.2.1.1 Elevation

A topographic land survey has been carried out in the area of interest. I used the resulting points to create a DTM with a horizontal resolution of 30 m by interpolating the values between the surveyed points using Regularized Spline with Tension (Mitášová and Hofierka, 1993; Mitášová and Mitáš, 1993) with the *v.surf.rst* tool from GRASS. The area of interest measures 53 km^2. Figure 4.13 shows the obtained DTM.

Figure 4.12: Location of Kolkata in India. The red polygon represents the study area

4.2.1.2 Rainfall

The rainfall for this event has been measured using the automated system described by Sen (2013). For this event, 4 rain-gauges where operational. The temporal resolution of the data is 15 min. A raster map has been created at each time step using the Inverse Distance Weighting method with a power coefficient of 3. Then, the generated raster maps have been referenced in a GRASS Space-Time Raster Dataset to be used in *Itzï*. Figure 4.14 show the total precipitated height during the 48 h event.

4.2.1.3 Water level at pumping stations

The water level of the pumping pits of three main pumping stations are recorded using the same infrastructure as the rainfall (Sen, 2013). Figure 4.15 shows the position of those stations within the drainage network, while Fig. 4.16 shows the evolution of the water level at those stations

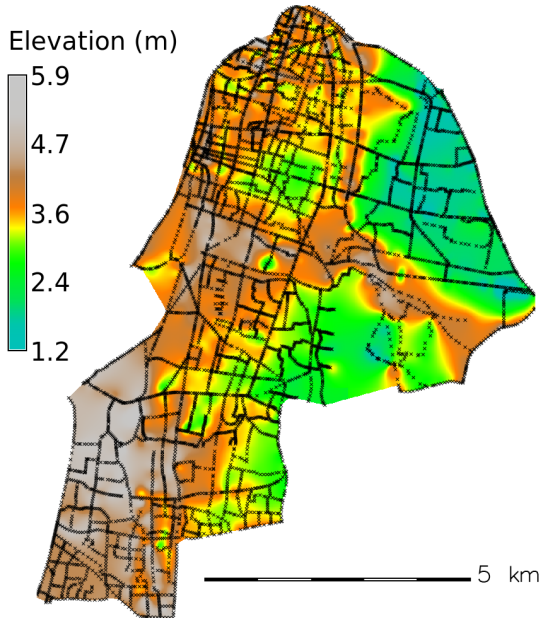

Figure 4.13: DTM of the area of interest of Kolkata. The black dots represent the points measured by land survey.

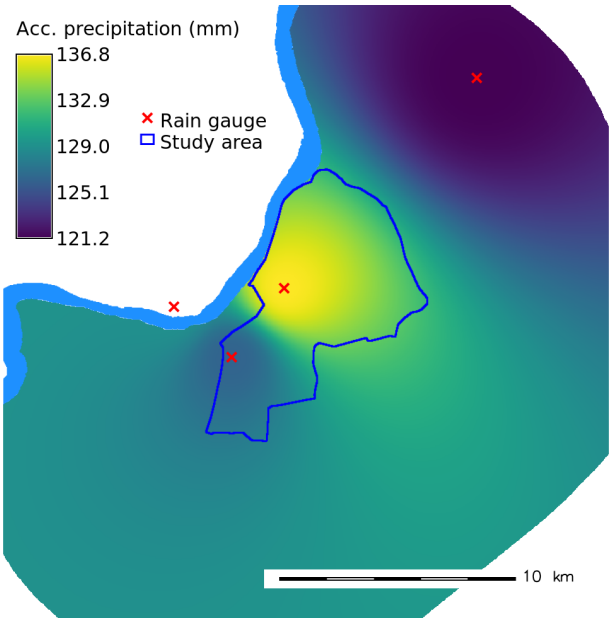

Figure 4.14: Accumulated rainfall during the 48 h event and location of the rain gauges used.

during the event.

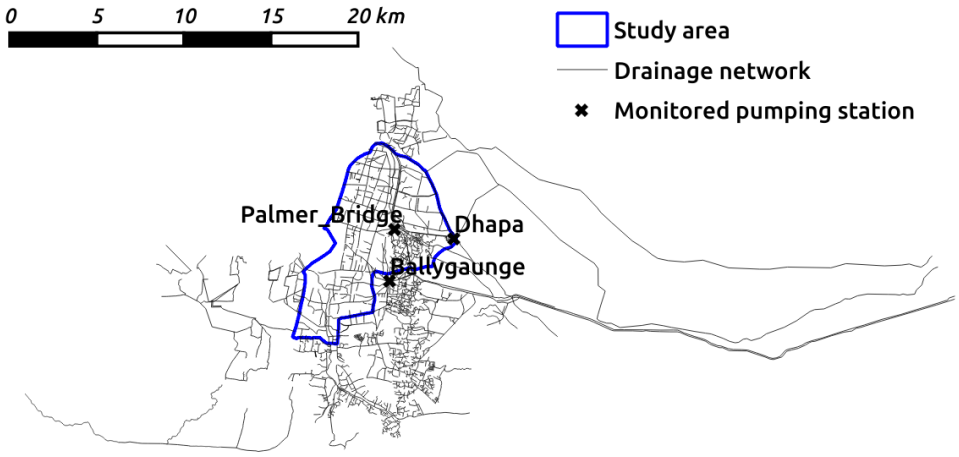

Figure 4.15: Overview of Kolkata's drainage network.

4.2.1.4 Drainage network

The first drainage of Kolkata has been laid out 140 years ago by the British authorities when the city, then known as Calcutta, was the capital of British India (Sen, 2013). Although Kolkata lies on the Hooghly river, most of its run-off and sewage waters are drained eastward through overland canals to a tidal creek known locally as Kultigang (Sen, 2013). Those canals are protected with gates that prevent the introduction of backwater in high tides. Only a small portion of the drainage network of the study area actually drains to the Hooghly (Sen, 2013). Due to the length of those canals (around 30 km) and the presence of tide gates, the tidal influence could be safely ignored as a first estimate (Dhrubajyoti Sen, personal communication, 4 March 2017).

The drainage network is available in the form of a SWMM input file. It comprises 2673 nodes and 2686 links. This includes pipes, open channels, pumping stations, reservoir etc. A Python tool has been developed to import the SWMM file into a GRASS vector file, with the attributes stored in the corresponding database tables. This allow to easily visualize the network together with the other geographical data, as shown in Fig. 4.15.

After comparison with the DTM, it appears that the invert elevation of 69 drainage junctions where situated over ground. The location of

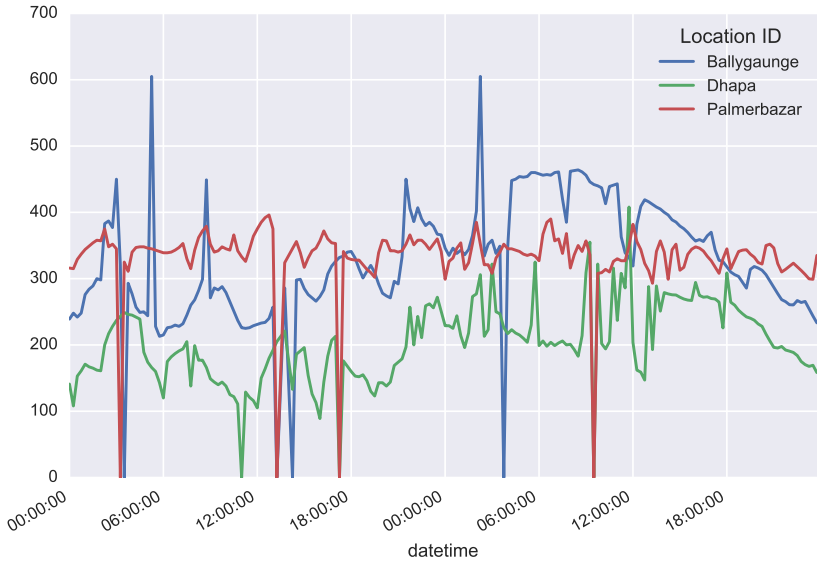

Figure 4.16: Measured water level in cm in the pumping stations during the event.

those junctions is shown on Fig. 4.17. The network has been modified to correct those inconsistencies. Furthermore, no indication was available about the pumps number, type, rating curve or operating rules at the pumping stations. Therefore, the measured water levels at three main pumping stations has been used as a downstream forcing and those pumping stations have not been modelled.

4.2.1.5 Flooded areas

Flooded areas for this event have been collected from the Facebook page of the Kolkata Traffic Police, which posted information about the affected zones. The identified roads are shown in Fig. 4.18.

In addition to the location, the dataset includes an approximation of the observed water depth classified according to lower body parts, namely the ankle and the knee. The average height of inhabitants of West Bengal between 20 and 49 years is 163.2 cm for men and 150.5 cm for women (Mamidi et al., 2011). The average relative knee height of inhabitant of Beijing is 29.7 % of total body height for the women, and 29.8 % for

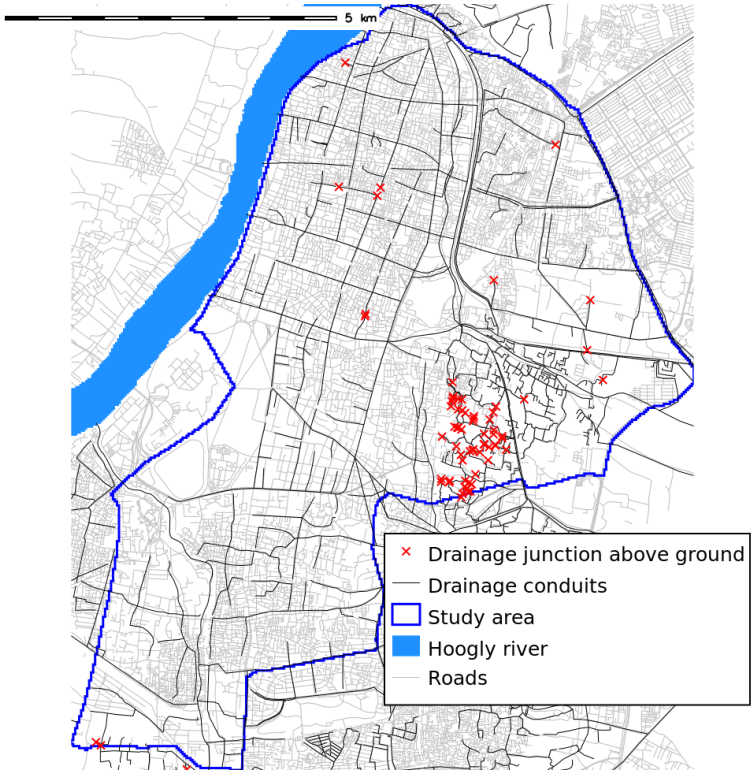

Figure 4.17: View of Kolkata's drainage network highlighting the junctions which invert elevation is located above ground level.

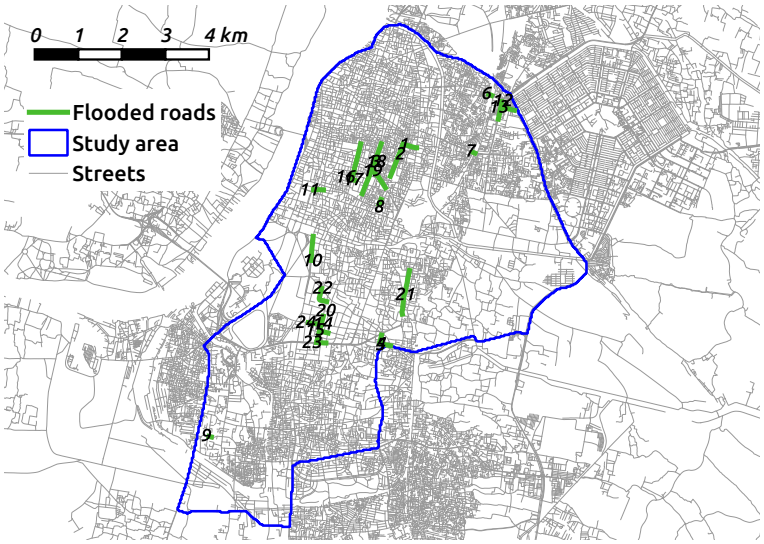

Figure 4.18: Roads identified as flooded by the Kolkata Traffic Police.

the men (D. J. Hunter et al., 2005). I will here consider that there is no significant variation of this proportion between the two countries. Considering a equal proportion of males and females, I can therefore estimate that the average knee height of the inhabitants of West Bengal is 46.7 cm. To take into account the uncertainty of this estimation, I arbitrarily associate a confidence interval of 5 cm. I have not found anthropometrics information about ankle height, so it is estimated here to be 10 cm. Table 4.7 recapitulates the results of this estimation process.

Table 4.7: Relation between observed water depth classes and estimated water depth.

Observed water depth class	Estimated water depth (m)
Above ankle deep	$0.10 < d < 0.47$
Knee deep	0.47 ± 0.05

4.2.2 Results

To simulations are run. One without drainage and another one with the drainage. The simulations are run for 48 h. The surface-drainage integration is done on every junction nodes that falls inside the raster computational region. Table 4.8 shows the computation times for each of those simulations. It can be noted that including the drainage has an important cost on the computation time. To understand better the difference in computation time, I performanced an analysis using a profiler. It results that the main computational cost when running the coupled model is not the actual drainage computation but the process of writing the results as vector maps and to populate the related DB tables. It is likely a limitation of GRASS and/or the type of DB back-end being used. Here I used SQLite, the GRASS default.

Figure 4.19 displays the maximum water levels attained during the simulation when the drainage is used. The flooded areas are spread over the study area. However, the larger depths are calculated in the south-east, where the water reaches depth above 1 m. This area is where most of the above-ground junctions where located (see Figure 4.17). Since the area is not identified as flooded in the police reports (see Figure 4.18), it might be the DEM in the area that is faulty, and not the drainage network

Table 4.8: Computation times with and without drainage for a 48 hours event.

Case	Computation time (hh:mm:ss)
Without drainage	00:03:05
With drainage	00:39:45

model, as first thought. It is however difficult to determine the real reason with the data at hand.

The differences due to the inclusion of the drainage network in the simulation are shown in Figure 4.20. Adding the drainage network into the simulation reduces the water depths up to more than 0.10 m (98th percentile: 0.14 m). The zone that shows the more changes is located in the north-east of the study area.

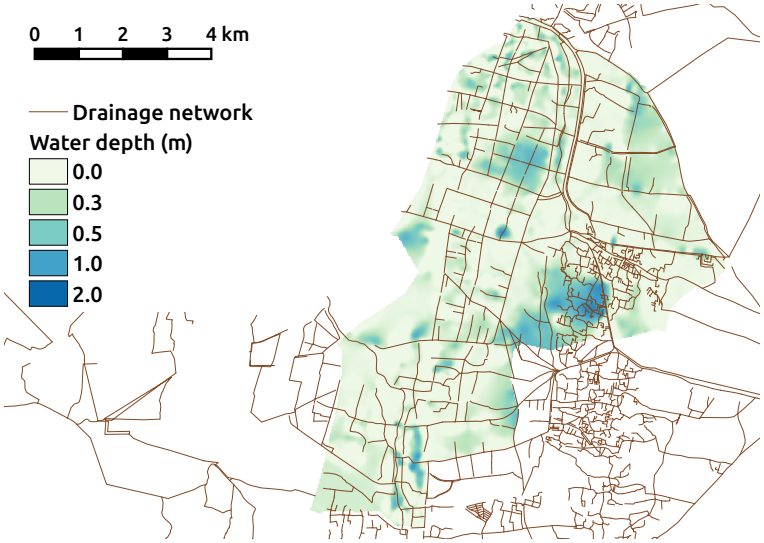

Figure 4.19: Maxima water depths obtained during the event when using the drainage network.

Now I compare the resulting maxima depths to the observed flooded roads. Given the subjective nature of the observations, the flood prediction at each observed street is categorised as 'good' or 'bad' if the computed maximum, mean or median along the given road is inside the given threshold. Tables 4.9 and 4.10 display the result of this work with and

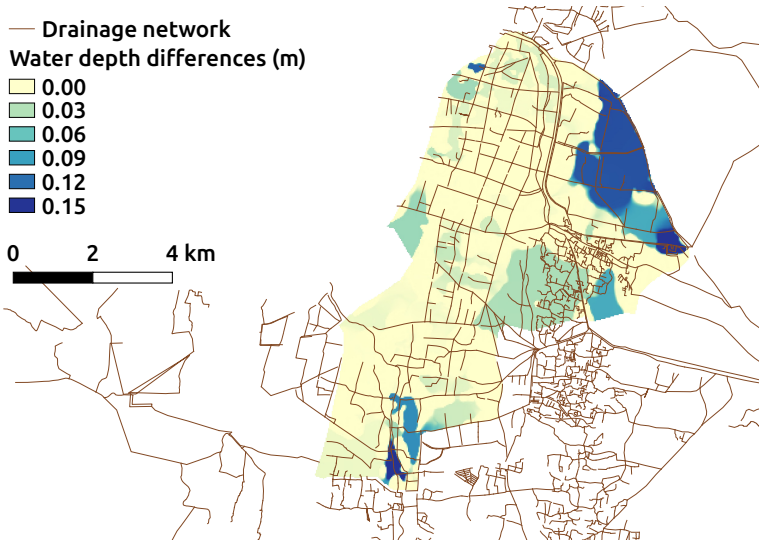

Figure 4.20: Differences in maximum water depth when the drainage is included or not. This is the additional water depth that occurs when the drainage is not included.

without drainage, respectively. With drainage, 10 observations out of 24, or 42 %, are adequately predicted by the numerical model. If the drainage network is not included, the number of correct observations drop to 9, or 38 %. The use of the coupled model does increases the performance of the numerical simulation, although slightly. Furthermore, I considered that the observations where made at the maximum water depth. There is no indication that this assumption might be true. It is more likely that the reports from police officer on the ground where made during a lapse of time and at various stages of the flooding event.

The results might not seems of high quality (only 42 % of correct predictions), however the uncertainties in the entry data should be taken into account. Those uncertainties could be summarized as follow:

- Inadecuate representation of flow pattern:
  - The DEM has a resolution of only 30 m, which is not enough to represent the narrow streets of Kolkata.
  - Building blockage are not considered.
- Drainage network model:
  - Some pipes shown to be over ground level (although it could be a DEM problem).
  - The georeferencing is crude, with many pipes not represented

under the roads as they should be.
  - Lack of information about the rules of operations of the numerous pumping stations; those stations play an important role in the drainage of Kolkata.
- Observations:
  - The observations are likely partials. Other flooded parts of the city might not be reported.
  - The reported values are subjective and numerical values must be infered.
  - The time at which the observations are made is not known. It is likely that they are not all made at the same time, and that they do not represent the water depth at its peak.

Table 4.9: Comparison between the observed water levels and the maximum computed depths *with* drainage. The statistics denote the variation of computed value along the given street. Observation number shown in Fig. 4.18

#	Observed water depth (m)		Max. computed water depth (m)			Prediction quality
	Low	High	Maximum	Mean	Median	
1	0.42	0.52	0.173034	0.153963	0.154557	Bad
2	0.42	0.52	0.757334	0.581923	0.628378	Bad
3	0.42	0.52	0.500112	0.372848	0.382104	Good
4	0.10	0.47	0.704026	0.665762	0.656357	Bad
5	0.42	0.52	0.668125	0.636484	0.642131	Bad
6	0.10	0.47	0.718474	0.640574	0.717205	Bad
7	0.42	0.52	0.463799	0.358191	0.358191	Good
8	0.42	0.52	0.110591	0.061683	0.050542	Bad
9	0.10	0.47	0.242456	0.226611	0.226611	Good
10	0.42	0.52	0.069052	0.016448	0.011440	Bad
11	0.10	0.47	0.007700	0.004697	0.005157	Bad
12	0.10	0.47	0.558103	0.514451	0.510847	Bad
13	0.10	0.47	0.509349	0.342319	0.388193	Good
14	0.42	0.52	0.108023	0.071948	0.078304	Bad
15	0.42	0.52	0.136153	0.053478	0.027736	Bad
16	0.10	0.47	0.267438	0.264642	0.267172	Good
17	0.10	0.47	0.499964	0.262533	0.202840	Good
18	0.10	0.47	0.543341	0.290709	0.373015	Good
19	0.10	0.47	0.497496	0.458792	0.476385	Good
20	0.42	0.52	0.102362	0.024191	0.009086	Bad
21	0.10	0.47	0.425738	0.238075	0.220619	Good
22	0.10	0.47	0.217732	0.114594	0.144956	Good
23	0.42	0.52	0.327600	0.239993	0.236212	Bad
24	0.42	0.52	0.201602	0.108574	0.094321	Bad

Table 4.10: Comparison between the observed water levels and the maximum computed depths *without* drainage. The statistics denote the variation of computed value along the given street. Observation number shown in Fig. 4.18

#	Observed water depth (m)		Max. computed water depth (m)			Prediction quality
	Low	High	Maximum	Mean	Median	
1	0.42	0.52	0.164226	0.145420	0.145876	Bad
2	0.42	0.52	0.748361	0.573011	0.619410	Bad
3	0.42	0.52	0.491064	0.363738	0.373050	Good
4	0.10	0.47	0.735853	0.697488	0.688139	Bad
5	0.42	0.52	0.699620	0.668021	0.673629	Bad
6	0.10	0.47	0.859275	0.781259	0.857786	Bad
7	0.42	0.52	0.594247	0.488594	0.488594	Good
8	0.42	0.52	0.101277	0.058698	0.052882	Bad
9	0.10	0.47	0.239200	0.223253	0.223253	Good
10	0.42	0.52	0.096160	0.019495	0.011392	Bad
11	0.10	0.47	0.007686	0.004660	0.005112	Bad
12	0.10	0.47	0.694503	0.652780	0.648476	Bad
13	0.10	0.47	0.647427	0.479943	0.526335	Bad
14	0.42	0.52	0.110358	0.074844	0.082680	Bad
15	0.42	0.52	0.136817	0.054914	0.029274	Bad
16	0.10	0.47	0.258231	0.255422	0.257961	Good
17	0.10	0.47	0.490720	0.253201	0.193582	Good
18	0.10	0.47	0.534298	0.283554	0.363886	Good
19	0.10	0.47	0.488443	0.449720	0.467335	Good
20	0.42	0.52	0.103055	0.024335	0.009039	Bad
21	0.10	0.47	0.458363	0.270561	0.253362	Good
22	0.10	0.47	0.233882	0.125406	0.159905	Good
23	0.42	0.52	0.331334	0.243646	0.239987	Bad
24	0.42	0.52	0.205712	0.111335	0.095211	Bad

5 Conclusion

In this work, I presented the development and implementation of a new numerical flood model. This software, named Itzï, combines a simplified surface flow model with the well-known SWMM drainage network model. The bi-directional interchanges between the two models is achieved by using a combination of weir and orifices equations. Itzï is released under a GPL license that allows its modification and unlimited use. Its implementation could therefore be studied by both scientists and engineers, and its use is free of charge. The numerical tool is the first FOSS of its kind, which makes it a great asset for the flood modelling community.

The surface model proved its ability to reproduce urban flood events, achieving correct predictions of water depth and arrival time of the flood wave. Indeed, numerical results compare very well against both analytic solutions of the SWE and LISFLOOD-FP, a well-proven flood model working with the same set of equations and assumptions.

The surface-drainage coupled model was tested using a published synthetic simplified test case. The numerical results from Itzï were comparable to those obtained using well-known commercial models. This result provided a solid step forward towards the application of Itzï to reproduce and characterise real urban floods.

Nonetheless, the use of a real flood event with all the required data at an adequate spatial and temporal resolution resulted elusive. Despite this fact, a real flood event registered in the city of Kolkata in 2015 was incorporated as a test case. Information relative to the sewer network and flood depths in several streets of the city was available. However, it should be noted that although this test case corresponded to a real city and flood, the quality of the information that was acquired was not optimal. For instance, the DEM was interpolated from a land survey, which resulted in a low level of information between the measured points. Indeed, compared to a 1d drainage model like SWMM, the additional com-

plexity of a coupled model requires data of higher quality. Those should include spatial distribution of rainfall within the catchment (e.g. from a dense network of rain gauges or weather radar), a DTM at a resolution related to the width of the streets (e.g. LiDAR data), land use information, and detailed sewer system data. A key lesson that can be learned from this test case is that there are a great number of uncertainties, not only in the proper modelling of urban floods, but in the data itself. Despite this fact, the model was able to identify the flooded areas registered by the police, and performed better with the integration of the drainage than with the surface model only.

We do recognise that the uncertainties associated to this test case prevents its use to adequately evaluate the capacity of the coupled model to represent real-world events. However, the lack of drainage network information at a proper level (e.g. primary and secondary lines), and to a lesser extend elevation data, is very common all over the word, especially in developing countries. From that perspective, the case of Kolkata could be classified as data-rich with its combination of multiple rain gauges at a decent temporal resolution, drainage monitoring stations, and the availability of a drainage network model.

Pluvial flooding in cities occurs when the local drainage system is not able to cope with the collection and conveying of surface runoff. Simultaneous modelling of all surface flow processes coupled with a pipe network is considered the more realistic approach to this problem. The exchange of water between the drainage model and the surface flow model is carried out via conceptual links representing inlets and manholes. The parameters of these links are another source of uncertainty in the modelling of urban floods, because of their complex geometry and flow regimes.

An obvious next step for improving Itzï is to build upon the recent advances in physical modelling of the interactions between a drainage network and a surface flume (Hakiel and Szydłowski, 2017; Rubinato et al., 2017). Using the results from such experiments as benchmarks will allow to 1) assess the capacity of Itzï to accurately model the interactions between a drainage network and a surface model, and 2) have an approach of the range of acceptable values that could be used to calibrate a coupled model in a real-world event.

Moving forward, the current software implementation of the coupling could be simplified. The likely future of Itzï is to become more modular and make use of existing software libraries that would be modified to permit the coupling. The Open Water Analytics community is maintaining

both a version of SWMM with additional API functions[1] and pyswmm, a Python interface that wrap this API[2]. Those packages were still in their infancy when the work on the Itzï coupling started. However, they vastly improved in the last two years and they are now a viable solution to base the drainage part of Itzï on. The objectives would be to 1) modify SWMM to integrate the coupling flow computation, 2) integrate those changes into pyswmm, 3) replace the current coupling code of Itzï to use pyswmm instead. Of the above, the points 1 and 2 are mostly coded, with the modification of SWMM awaiting approval for merging[3] and the changes to pyswmm being well under way[4]. The expected outcomes of those changes to Itzï will be three-fold. First, the codebase will be smaller and easier to comprehend. Second, the maintenance and documentation of the drainage code will be shared among a wider community. Finally, a performance improvement is likely to occur with the implantation of the coupling directly inside the SWMM code.

[1] `https://github.com/OpenWaterAnalytics/Stormwater-Management-Model`

[2] `https://github.com/OpenWaterAnalytics/pyswmm`

[3] `https://github.com/OpenWaterAnalytics/Stormwater-Management-Model/pull/124`

[4] `https://github.com/lrntct/pyswmm/tree/surfaceCoupling`

Bibliography

Adams, J. M., N. M. Gasparini, D. E. J. Hobley, G. E. Tucker, E. W. H. Hutton, S. S. Nudurupati and E. Istanbulluoglu (2017). 'The Landlab v1.0 OverlandFlow component: a Python tool for computing shallow-water flow across watersheds'. English. In: *Geoscientific Model Development* 10.4, pp. 1645–1663. ISSN: 1991-9603. DOI: 10.5194/gmd-10-1645-2017.

Almeida, G. A. M. de and P. D. Bates (2013). 'Applicability of the local inertial approximation of the shallow water equations to flood modeling'. In: *Water Resources Research* 49.8, pp. 4833–4844. ISSN: 00431397. DOI: 10.1002/wrcr.20366.

Almeida, G. A. M. de, P. D. Bates, J. E. Freer and M. Souvignet (2012). 'Improving the stability of a simple formulation of the shallow water equations for 2-D flood modeling'. In: *Water Resources Research* 48.5, pp. 1–14. ISSN: 00431397. DOI: 10.1029/2011WR011570.

Almejo, R. and Y. Téllez (2015). 'Cambio demográfico en la Zona Metropolitana del Valle de México, 2000-2010'. In: *La Situación Demográfica de México 2015*. Consejo Nacional de población, pp. 197–227. URL: http://conapo.gob.mx/en/CONAPO/Cambio%7B%5C_%7Ddemografico%7B%5C_%7Den%7B%5C_%7Dla%7B%5C_%7DZona%7B%5C_%7DMetropolitana%7B%5C_%7Ddel%7B%5C_%7DValle%7B%5C_%7Dde%7B%5C_%7DMexico%7B%5C_%7D2000%7B%5C_%7D2010.

Animal Político (2016). *En menos de 7 días, la lluvia causa el cierre dos veces del Metro de la CDMX*. URL: http://www.animalpolitico.com/2016/09/encharcamientos-cdmx-metro-lluvia/ (visited on 29/01/2018).

— (2017). *Inundaciones y granizo azotan la Ciudad de México*. URL: http://www.animalpolitico.com/2017/06/inundaciones-y-granizo-ciudad-de-mexico/ (visited on 29/01/2018).

Arnaud, P., C. Bouvier, L. Cisneros and R. Domínguez-Mora (2002). 'Influence of rainfall spatial variability on flood prediction'. In: *Journal of Hydrology*. ISSN: 00221694. DOI: 10.1016/S0022-1694(01)00611-4.

Aronica, G. T. and L. G. Lanza (2005). 'Drainage efficiency in urban areas: A case study'. In: *Hydrological Processes* 19.5, pp. 1105–1119. ISSN: 08856087. DOI: 10.1002/hyp.5648. URL: http://doi.wiley.com/10.1002/hyp.5648.

Baker, M. (2016). 'Is there a reprodicibility crisis?' In: *Nature* 533, pp. 452–. URL: http://www.gulfcoastconsortia.org/wp-content/uploads/2017/01/Ellis-533452-1.pdf.

Bates, P. D. and A. P. J. De Roo (2000). 'A simple raster-based model for flood inundation simulation'. In: *Journal of hydrology* 236.1, pp. 54–77.

Bates, P. D., M. S. Horritt and T. J. Fewtrell (2010). 'A simple inertial formulation of the shallow water equations for efficient two-dimensional flood inundation modelling'. In: *Journal of Hydrology* 387.1-2, pp. 33–45. ISSN: 00221694. DOI: 10.1016/j.jhydrol.2010.03.027. URL: http://dx.doi.org/10.1016/j.jhydrol.2010.03.027.

Bazin, P.-H., H. Nakagawa, K. Kawaike, A. Paquier and E. Mignot (2014). 'Modeling flow exchanges between a street and an underground drainage pipe during urban floods'. In: *Journal of Hydraulic Engineering* 140.10. DOI: http://dx.doi.org/10.1061/(ASCE)HY.1943-7900.0000917.

Behnel, S., R. Bradshaw, C. Citro, L. Dalcin, D. S. Seljebotn and K. Smith (2011). 'Cython: The Best of Both Worlds'. In: *Computing in Science Engineering* 13.2, pp. 31–39. ISSN: 1521-9615. DOI: 10.1109/MCSE.2010.118.

Beven, K. J. (2012). *Rainfall-runoff modelling : the primer*. Wiley-Blackwell, p. 457. ISBN: 047071459X.

Bradbrook, K. F., S. Lane, S. Waller and P. D. Bates (2004). 'Two dimensional diffusion wave modelling of flood inundation using a simplified channel representation'. In: *International Journal of River Basin Management* 2.3, pp. 211–223. ISSN: 1571-5124. DOI: 10.1080/15715124.2004.9635233.

Bruni, G., R. Reinoso, N. van de Giesen, F. H. L. R. Clemens and J. A. E. Ten Veldhuis (2015). 'On the sensitivity of urban hydrodynamic modelling to rainfall spatial and temporal resolution'. In: *Hydrology and Earth System Sciences* 19.2. ISSN: 16077938. DOI: 10.5194/hess-19-691-2015.

Carr, R. and G. Smith (2007). 'Linking of 2D and Pipe hydraulic models at fine spatial scales'. In: *Water Practice and Technology* 2.2.

Chen, A. S., S. Djordjević, J. Leandro and D. A. Savić (2007). 'The urban inundation model with bidirectional flow interaction between 2D overland surface and 1D sewer networks'. In: *Novatech 2007*. Lyon, France, pp. 465–472. DOI: 2042/25250.

Chen, A. S., M. Hsu, T. S. Chen and T. J. Chang (2005). 'An integrated inundation model for highly developed urban areas'. In: *Water Science and Technology* 51.2, pp. 221–229. ISSN: 02731223. URL: http://www.ncbi.nlm.nih.gov/pubmed/15790247.

Chen, A. S., J. Leandro and S. Djordjević (2015). 'Modelling sewer discharge via displacement of manhole covers during flood events using 1D/2D SIPSON/P-DWave dual drainage simulations'. In: *Urban Water Journal* 9006.August, pp. 1–11. ISSN: 1573-062X. DOI: 10.1080/1573062X.2015.1041991. URL: http://www.tandfonline.com/doi/full/10.1080/1573062X.2015.1041991.

Chen, J., J. Chen, A. Liao, X. Cao, L. Chen, X. Chen, C. He, G. Han, S. Peng, M. Lu, W. Zhang, X. Tong and J. Mills (2014). 'Global land cover mapping at 30m resolution: A POK-based operational approach'. In: *ISPRS Journal of Photogrammetry and Remote Sensing* 103, pp. 7–27. ISSN: 09242716. DOI: 10.1016/j.isprsjprs.2014.09.002. URL: http://www.sciencedirect.com/science/article/pii/S0924271614002275.

Chiles, J.-P. and P. Delfiner (2012). *Geostatistics : modeling spatial uncertainty*. John Wiley & Sons, p. 726. ISBN: 9781118136171.

Chocat, B., P. Krebs, J. Marsalek, W. Rauch and W. Schilling (2001). 'Urban drainage redefined: from stormwater integrated management'. In: *Water Science and Technology* 43.5, pp. 61–68. ISSN: 02731223. URL: http://wst.iwaponline.com/content/43/5/61.

Chow, V. T. (1959). *Open channel hydraulics*. McGraw-Hill Book Company, Inc; New York.

Cook, A. and V. Merwade (2009). 'Effect of topographic data, geometric configuration and modeling approach on flood inundation mapping'. In: *Journal of Hydrology* 377.1-2, pp. 131–142. ISSN: 00221694. DOI: 10.1016/j.jhydrol.2009.08.015. URL: http://linkinghub.elsevier.com/retrieve/pii/S0022169409004909.

Costabile, P., C. Costanzo and F. Macchione (2017). 'Performances and limitations of the diffusive approximation of the 2-d shallow water equations for flood simulation in urban and rural areas'. In: *Applied*

Numerical Mathematics 116, pp. 141–156. ISSN: 0168-9274. DOI: 10.1016/J.APNUM.2016.07.003. URL: https://www.sciencedirect.com/science/article/pii/S0168927416301106?via%7B%5C%%7D3Dihub.

Coulthard, T. J. and L. Frostick (2010). 'The Hull floods of 2007: implications for the governance and management of urban drainage systems'. In: *Journal of Flood Risk Management* 3.3, pp. 223–231. ISSN: 1753318X. DOI: 10.1111/j.1753-318X.2010.01072.x. URL: http://doi.wiley.com/10.1111/j.1753-318X.2010.01072.x.

Courty, L. G. and A. Pedrozo-Acuña (2016a). 'A GRASS GIS module for 2D superficial flow simulations'. In: *Proceedings of the 12th International Conference on Hydroinformatics*. DOI: 10.5281/zenodo.159617.

— (2016b). 'Modelo numérico para la simulación dinámica de inundaciones urbanas en SIG'. In: *Proceedings of XXVII Congreso Latinoamericano de Hidráulica*. DOI: 10.5281/zenodo.159619.

Courty, L. G., A. Pedrozo-Acuña and P. D. Bates (2017). 'Itzï (version 17.1): an open-source, distributed GIS model for dynamic flood simulation'. In: *Geoscientific Model Development* 10.4, pp. 1835–1847. DOI: 10.5194/gmd-10-1835-2017. URL: http://www.geosci-model-dev.net/10/1835/2017/.

Courty, L. G., M. Á. Rico-Ramirez and A. Pedrozo-Acuña (2018). 'The Significance of the Spatial Variability of Rainfall on the Numerical Simulation of Urban Floods'. In: *Water* 10.2, p. 207. DOI: 10.3390/W10020207. URL: http://www.mdpi.com/264172.

Cressie, N. (2015). *Statistics for spatial data*. Revised Ed. John Wiley & Sons, p. 928. ISBN: 9781119115175.

Cristiano, E., M.-c. ten Veldhuis and N. van de Giesen (2017). 'Spatial and temporal variability of rainfall and their effects on hydrological response in urban areas – a review'. In: *Hydrology and Earth System Sciences* 21.7, pp. 3859–3878. ISSN: 1607-7938. DOI: 10.5194/hess-21-3859-2017. URL: https://www.hydrol-earth-syst-sci.net/21/3859/2017/.

Delestre, O., S. Cordier, F. Darboux, M. Du, F. James, C. Laguerre, C. Lucas and O. Planchon (2014). 'FullSWOF: A Software for Overland Flow Simulation'. In: *Advances in Hydroinformatics*. Singapore: Springer Singapore, pp. 221–231. DOI: 10.1007/978-981-4451-42-0_19. URL: http://link.springer.com/10.1007/978-981-4451-42-0%7B%5C_%7D19.

Delestre, O., C. Lucas, P.-A. Ksinant, F. Darboux, C. Laguerre, T.-N.-T. Vo, F. James and S. Cordier (2013). 'SWASHES: a compilation of shal-

low water analytic solutions for hydraulic and environmental studies'. en. In: *International Journal for Numerical Methods in Fluids* 72.3, pp. 269–300. ISSN: 02712091. DOI: 10.1002/fld.3741. URL: https://hal.archives-ouvertes.fr/hal-00628246.

Di Baldassarre, G. (2012). 'Data sources'. In: *Floods in a Changing Climate: Inundation Modelling*. Cambridge: Cambridge University Press, pp. 33–42. DOI: 10.1017/CBO9781139088411.008. URL: http://ebooks.cambridge.org/ref/id/CBO9781139088411A013.

Djordjević, S., D. Prodanović and Č. Maksimović (1999). 'An approach to simulation of dual drainage'. In: *Water Science and Technology* 39.9, pp. 95–103. ISSN: 0273-1223. DOI: 10.1016/S0273-1223(99)00221-8.

Djordjević, S., A. J. Saul, G. R. Tabor, J. Blanksby, I. Galambos, I. Sabtu and G. Sailor (2011). 'Experimental and numerical investigation of interactions between above and below ground drainage systems'. In: *12th International Conference on Urban Drainage* 1999.September, pp. 10–15.

Dobbs, R., S. Smit, J. Remes, J. Manyika, C. Roxburgh and A. Restrepo (2011). *Urban world: Mapping the economic power of cities*. McKinsey Global Institute, p. 62. ISBN: 0983179662. URL: http://www.mckinsey.com/insights/urbanization/urban%7B%5C_%7Dworld.

Domínguez-Mora, R. (2000). 'Las Inundaciones en la Ciudad de Mexico. Problematica y Alternativas de Solucion'. In: *Revista Digital Universitaria* 1.2. URL: http://www.revista.unam.mx/vol.1/num2/proyec1/index.html.

Elliott, A. and S. Trowsdale (2007). 'A review of models for low impact urban stormwater drainage'. In: *Environmental Modelling & Software* 22.3, pp. 394–405. ISSN: 1364-8152. DOI: 10.1016/J.ENVSOFT.2005.12.005. URL: http://www.sciencedirect.com/science/article/pii/S1364815206000053.

Ercan, M. B. and J. L. Goodall (2013). 'Estimating Watershed-Scale Precipitation by Combining Gauge- and Radar-Derived Observations'. In: *Journal of Hydrologic Engineering* 18.8, pp. 983–994. ISSN: 1084-0699. DOI: 10.1061/(ASCE)HE.1943-5584.0000687. URL: http://ascelibrary.org/doi/10.1061/%7B%5C%%7D28ASCE%7B%5C%%7D29HE.1943-5584.0000687.

Fewtrell, T. J., A. Duncan, C. C. Sampson, J. C. Neal and P. D. Bates (2011). 'Benchmarking urban flood models of varying complexity and scale

using high resolution terrestrial LiDAR data'. In: *Physics and Chemistry of the Earth* 36.7, pp. 281–291.

Fraga, I., L. Cea and J. Puertas (2017). 'Validation of a 1D-2D dual drainage model under unsteady part-full and surcharged sewer conditions'. In: *Urban Water Journal* 14.1, pp. 74–84. ISSN: 17449006. DOI: 10.1080/1573062X.2015.1057180. URL: https://www.tandfonline.com/doi/full/10.1080/1573062X.2015.1057180.

Free Software Fundation (2016). *The Free Software Definition*. URL: https://www.gnu.org/philosophy/free-sw.html (visited on 18/01/2018).

García Cortés, A. and F. Hernández Serrano (1975). 'Atlas de planos tecnicos e historicos'. In: *Memoria de las obras del sistema de drenaje profundo del Distrito Federal*. DDF. Chap. 4.

Gebbert, S. and E. J. Pebesma (2014). 'TGRASS: A temporal GIS for field based environmental modeling'. In: *Environmental Modelling & Software* 53, pp. 1–12.

Gires, A., C. Onof, C. Maksimovic, D. Schertzer, I. Tchiguirinskaia and N. Simoes (2012). 'Quantifying the impact of small scale unmeasured rainfall variability on urban runoff through multifractal downscaling: A case study'. In: *Journal of Hydrology* 442-443, pp. 117–128. ISSN: 00221694. DOI: 10.1016/j.jhydrol.2012.04.005. URL: http://www.sciencedirect.com/science/article/pii/S0022169412002685%7B%5C#%7Db0005.

Goudenhoofdt, E. and L. Delobbe (2009). 'Evaluation of radar-gauge merging methods for quantitative precipitation estimates'. In: *Hydrology and Earth System Sciences* 13.2, pp. 195–203. ISSN: 1607-7938. DOI: 10.5194/hess-13-195-2009. URL: http://www.hydrol-earth-syst-sci.net/13/195/2009/.

Grant, G. E. (1997). 'Critical flow constrains flow hydraulics in mobile-bed streams: A new hypothesis'. In: *Water Resources Research* 33.2, pp. 349–358. ISSN: 00431397. DOI: 10.1029/96WR03134. URL: http://doi.wiley.com/10.1029/96WR03134.

Haberlandt, U. (2007). 'Geostatistical interpolation of hourly precipitation from rain gauges and radar for a large-scale extreme rainfall event'. In: *Journal of Hydrology* 332.1-2, pp. 144–157. ISSN: 00221694. DOI: 10.1016/j.jhydrol.2006.06.028. URL: http://www.sciencedirect.com/science/article/pii/S0022169406003416.

Hakiel, J. and M. Szydłowski (2017). 'Interaction between storm water conduit and surface flow for urban flood inundation modelling'. In: *International Journal of Sustainable Development and Planning* 12.01,

pp. 133–143. ISSN: 1743-7601. DOI: 10.2495/SDP-V12-N1-133-143. URL: http://www.witpress.com/journals/SDP-133-143.

Hallegatte, S., C. Green, R. J. Nicholls and J. Corfee-Morlot (2013). 'Future flood losses in major coastal cities'. In: *Nature climate change* 3.9, pp. 802–806. DOI: 10.1038/nclimate1979.

Harrison, D. L., R. W. Scovell and M. Kitchen (2009). 'High-resolution precipitation estimates for hydrological uses'. In: *Proceedings of the Institution of Civil Engineers - Water Management* 162.2, pp. 125–135. ISSN: 1741-7589. DOI: 10.1680/wama.2009.162.2.125. URL: http://www.icevirtuallibrary.com/doi/10.1680/wama.2009.162.2.125.

Harvey, H. and D. Han (2002). 'The relevance of open source hydroinformatics'. In: *Journal of Hydroinformatics* 04.JANUARY 2002, pp. 219–234. ISSN: 1464-7141.

Heber Green, W. and G. A. Ampt (1911). 'Studies on Soil Phyics.' English. In: *The Journal of Agricultural Science* 4.01, p. 1. ISSN: 0021-8596. DOI: 10.1017/S0021859600001441. URL: http://journals.cambridge.org/abstract%7B%5C_%7DS0021859600001441.

Hengl, T., J. Mendes de Jesus, G. B. M. Heuvelink, M. R. Gonzalez, M. Kilibarda, A. Blagotí, W. Shangguan, M. N. Wright, X. Geng, B. Bauer-Marschallinger, M. A. Guevara, R. Vargas, R. A. Macmillan, N. H. Batjes, J. G. B. Leenaars, E. Ribeiro, I. Wheeler, S. Mantel and B. Kempen (2017). 'SoilGrids250m: Global Gridded Soil Information Based on Machine Learning'. In: *PLOS One* 12, pp. 1–40. DOI: 10.1371/journal.pone.0169748.

Hernández-Espriú, A., J. A. Reyna-Gutiérrez, E. Sánchez-León, E. Cabral-Cano, J. Carrera-Hernández, P. Martínez-Santos, S. Macías-Medrano, G. Falorni and D. Colombo (2014). 'The DRASTIC-Sg model: an extension to the DRASTIC approach for mapping groundwater vulnerability in aquifers subject to differential land subsidence, with application to Mexico City'. In: *Hydrogeology Journal* 22.6, pp. 1469–1485. ISSN: 1431-2174. DOI: 10.1007/s10040-014-1130-4. URL: http://link.springer.com/10.1007/s10040-014-1130-4.

Hirabayashi, Y., R. Mahendran, S. Koirala, L. Konoshima, D. Yamazaki, S. Watanabe, H. Kim and S. Kanae (2013). 'Global flood risk under climate change'. In: *Nature Climate Change* 3.9, pp. 816–821. ISSN: 1758-678X. DOI: 10.1038/nclimate1911. URL: http://www.nature.com/doifinder/10.1038/nclimate1911.

Hodgson, M. E. and P. Bresnahan (2004). 'Accuracy of Airborne Lidar-Derived Elevation'. In: *Photogrammetric Engineering & Remote Sensing* 3, pp. 331–339. ISSN: 00991112. DOI: 10.14358/PERS.70.3.331.

Horritt, M. S. and P. D. Bates (2002). 'Evaluation of 1D and 2D numerical models for predicting river flood inundation'. In: *Journal of Hydrology* 268.1-4, pp. 87–99. ISSN: 00221694. DOI: 10.1016/S0022-1694(02)00121-X. URL: http://www.sciencedirect.com/science/article/pii/S002216940200121X.

Hsu, M., S. Chen and T. Chang (2000). 'Inundation simulation for urban drainage basin with storm sewer system'. In: *Journal of Hydrology* 234.1, pp. 21–37. ISSN: 00221694. DOI: 10.1016/S0022-1694(00)00237-7.

Hunter, D. J., J. Niu, Y. Zhang, M. C. Nevitt, L. Xu, L.-Y. Lui, W. Yu, P. Aliabadi, T. S. Buchanan and D. T. Felson (2005). 'Knee height, knee pain, and knee osteoarthritis: The Beijing Osteoarthritis Study'. In: *Arthritis & Rheumatism* 52.5, pp. 1418–1423. ISSN: 0004-3591. DOI: 10.1002/art.21017. URL: http://doi.wiley.com/10.1002/art.21017.

Hunter, N. M., P. D. Bates, S. Neelz, G. Pender, I. Villanueva, N. G. Wright, D. Liang, R. A. Falconer, B. Lin, S. Waller, A. J. Crossley and D. C. Mason (2008). 'Benchmarking 2D hydraulic models for urban flooding'. In: *Proceedings of the ICE - Water Management* 161.1, pp. 13–30. ISSN: 1741-7589. DOI: 10.1680/wama.2008.161.1.13. URL: http://eprints.whiterose.ac.uk/77249/.

IFRC (2016). *World Disasters Report 2016. Resilience : saving lives today, investing for tomorrow*, p. 282. ISBN: 9789291392407. URL: http://www.ifrc.org/en/publications-and-reports/world-disasters-report/world-disasters-report/.

INEGI (2012). *Zonas Metropolitanas de los Estados Unidos Mexicanos*.

Jahanbazi, M., I. Özgen, R. Aleixo and R. Hinkelmann (2017). 'Development of a diffusive wave shallow water model with a novel stability condition and other new features'. In: *Journal of Hydroinformatics* 19.3. URL: http://jh.iwaponline.com/content/19/3/405.

Jewell, S. A. and N. Gaussiat (2015). 'An assessment of kriging-based rain-gauge-radar merging techniques'. In: *Quarterly Journal of the Royal Meteorological Society* 141.691, pp. 2300–2313. ISSN: 00359009. DOI: 10.1002/qj.2522. URL: http://doi.wiley.com/10.1002/qj.2522.

Kent, K. M., D. E. Woodward, C. C. Hoeft, A. Humpal and G. Cerrelli (2010). 'Time of Concentration'. In: *National Engineering Handbook -*

Part 630 Hydrology. United States Departament of Agriculture. Chap. 15, p. 29.

Kishtawal, C. M., D. Niyogi, M. Tewari, R. A. Pielke and J. M. Shepherd (2010). 'Urbanization signature in the observed heavy rainfall climatology over India'. In: *International Journal of Climatology* 30.13, pp. 1908–1916. ISSN: 08998418. DOI: 10.1002/joc.2044. URL: http://doi.wiley.com/10.1002/joc.2044.

Klein Tank, A. M. G., J. B. Wijngaard, G. P. Können, R. Böhm, G. Demarée, A. Gocheva, M. Mileta, S. Pashiardis, L. Hejkrlik, C. Kern-Hansen, R. Heino, P. Bessemoulin, G. Müller-Westermeier, M. Tzanakou, S. Szalai, T. Pálsdóttir, D. Fitzgerald, S. Rubin, M. Capaldo, M. Maugeri, A. Leitass, A. Bukantis, R. Aberfeld, A. F. V. Van Engelen, E. Forland, M. Mietus, F. Coelho, C. Mares, V. Razuvaev, E. Nieplova, T. Cegnar, J. Antonio López, B. Dahlström, A. Moberg, W. Kirchhofer, A. Ceylan, O. Pachaliuk, L. V. Alexander and P. Petrovic (2002). 'Daily dataset of 20th-century surface air temperature and precipitation series for the European Climate Assessment'. In: *International Journal of Climatology* 22.12, pp. 1441–1453. ISSN: 08998418. DOI: 10.1002/joc.773. URL: http://www.ecad.eu.

Kloss, G. K. (2008). 'Automatic C Library Wrapping Ctypes from the Trenches'. In: *The Python Papers* 3.3, p. 5.

Leandro, J., A. S. Chen and A. Schumann (2014). 'A 2D Parallel Diffusive Wave Model for floodplain inundation with variable time step (P-DWave)'. In: *Journal of Hydrology* 517, pp. 250–259. DOI: 10.1016/j.jhydrol.2014.05.020.

Leandro, J. and R. Martins (2016). 'A methodology for linking 2D overland flow models with the sewer network model SWMM 5.1 based on dynamic link libraries'. In: *Water Science and Technology* 73.12, pp. 3017–3026. ISSN: 0273-1223. DOI: 10.2166/wst.2016.171. URL: http://wst.iwaponline.com/cgi/doi/10.2166/wst.2016.171.

Leandro, J., A. S. Chen, S. Djordjević and D. A. Savić (2009). 'Comparison of 1D/1D and 1D/2D coupled (sewer/surface) hydraulic models for urban flood simulation'. In: *Journal of hydraulic engineering* 135.6, pp. 495–504.

Leandro, J., S. Djordjević, A. S. Chen and D. A. Savić (2007). 'The use of multiple-linking-element for connecting surface and subsurface networks'. In: *32nd congress of IAHR - Harmonizing the Demand or Art and Nature in Hydraulics*. IAHR. Venice, Italy.

Leitão, J. P., N. E. Simões, R. D. Pina, S. Ochoa-Rodríguez, C. Onof and A. Sá Marques (2017). 'Stochastic evaluation of the impact of sewer inlets' hydraulic capacity on urban pluvial flooding'. In: *Stochastic Environmental Research and Risk Assessment* 31.8, pp. 1907–1922. ISSN: 14363259. DOI: 10.1007/s00477-016-1283-x. URL: http://link.springer.com/10.1007/s00477-016-1283-x.

Liguori, S. and M. A. Rico-Ramirez (2014). 'A review of current approaches to radar-based quantitative precipitation forecasts'. In: *International Journal of River Basin Management* 12.4, pp. 391–402. ISSN: 1571-5124. DOI: 10.1080/15715124.2013.848872. URL: http://www.tandfonline.com/doi/abs/10.1080/15715124.2013.848872.

Lopes, P., J. Leandro, R. Carvalho, P. Páscoa and R. Martins (2013). 'Numerical and experimental investigation of a gully under surcharge conditions'. en. In: *Urban Water Journal* 12.August 2015, pp. 1–9. ISSN: 1573-062X. DOI: 10.1080/1573062X.2013.831916. URL: http://dx.doi.org/10.1080/1573062X.2013.831916%20http://www.tandfonline.com/doi/full/10.1080/1573062X.2013.831916.

MacDonald, I., M. J. Baines, N. K. Nichols and P. G. Samuels (1997). 'Analytic Benchmark Solutions for Open-Channel Flows'. en. In: *Journal of Hydraulic Engineering* 123.11, pp. 1041–1045. ISSN: 0733-9429. DOI: 10.1061/(ASCE)0733-9429(1997)123:11(1041). URL: http://ascelibrary.org/doi/abs/10.1061/(ASCE)0733-9429(1997)123:11(1041).

Mamidi, R. S., B. Kulkarni and A. Singh (2011). 'Secular Trends in Height in Different States of India in Relation to Socioeconomic Characteristics and Dietary Intakes'. In: *Food and Nutrition Bulletin* 32.1, pp. 23–34. ISSN: 0379-5721. DOI: 10.1177/156482651103200103. URL: http://journals.sagepub.com/doi/10.1177/156482651103200103.

Mark, O., S. Weesakul, C. Apirumanekul, S. B. Aroonnet and S. Djordjević (2004). 'Potential and limitations of 1D modelling of urban flooding'. In: *Journal of Hydrology* 299.3-4, pp. 284–299. ISSN: 00221694. DOI: 10.1016/j.jhydrol.2004.08.014.

Martins, R., J. Leandro, A. S. Chen and S. Djordjević (2017). 'A comparison of three dual drainage models: Shallow Water vs Local Inertial vs Diffusive Wave'. In: *Journal of Hydroinformatics*. ISSN: 1464-7141. DOI: 10.2166/hydro.2017.075.

Met Office (2003). '1 km Resolution UK Composite Rainfall Data from the Met Office Nimrod System'. In: *NCAS British Atmospheric Data Centre*. URL: http://catalogue.ceda.ac.uk/uuid/27dd6ffba67f667a18c62de5c3456350.

Miller, J. D., H. Kim, T. R. Kjeldsen, J. Packman, S. Grebby and R. Dearden (2014). 'Assessing the impact of urbanization on storm runoff in a peri-urban catchment using historical change in impervious cover'. In: *Journal of Hydrology* 515, pp. 59–70. ISSN: 00221694. DOI: 10.1016/j.jhydrol.2014.04.011.

Mitášová, H. and J. Hofierka (1993). 'Interpolation by regularized spline with tension: II. Application to terrain modeling and surface geometry analysis'. In: *Mathematical Geology* 25.6, pp. 657–669. ISSN: 08828121. DOI: 10.1007/BF00893172.

Mitášová, H., M. Landa and M. Shukunobe (2012). 'Building open source geospatial education at research universities: Where we are and what is holding us back'. In: *Open Source Geospatial Research & Education Symposium*, pp. 42–49.

Mitášová, H. and L. Mitáš (1993). 'Interpolation by regularized spline with tension: I. Theory and implementation'. In: *Mathematical Geology* 25.6, pp. 641–655. ISSN: 08828121. DOI: 10.1007/BF00893171.

Moriasi, D., J. Arnold, M. Van Liew, R. Binger, R. Harmel and T. Veith (2007). 'Model evaluation guidelines for systematic quantification of accuracy in watershed simulations'. In: *Transactions of the ASABE* 50.3, pp. 885–900. ISSN: 0001-2351. DOI: 10.13031/2013.23153. arXiv: 0001âĹŠ2351. URL: http://swat.tamu.edu/media/1312/moriasimodeleval.pdf.

Mungkasi, S. and S. G. Roberts (2013). 'Validation of ANUGA hydraulic model using exact solutions to shallow water wave problems'. In: *Journal of Physics: Conference Series*. Vol. 423. 1. IOP Publishing, p. 012029. DOI: 10.1088/1742-6596/423/1/012029. URL: http://stacks.iop.org/1742-6596/423/i=1/a=012029?key=crossref.8aab96f1098154680703bf2648228a84.

Neal, J. C., T. J. Fewtrell, P. D. Bates and N. G. Wright (2010). 'A comparison of three parallelisation methods for 2D flood inundation models'. In: *Environmental Modelling & Software* 25.4, pp. 398–411.

Neal, J. C., G. J.-P. Schumann, T. J. Fewtrell, M. Budimir, P. D. Bates and D. Mason (2011). 'Evaluating a new LISFLOOD-FP formulation with data from the summer 2007 floods in Tewkesbury, UK'. In: *Journal of Flood Risk Management* 4.2, pp. 88–95. ISSN: 1753318X. DOI: 10.1111/j.1753-318X.2011.01093.x. URL: http://doi.wiley.com/10.1111/j.1753-318X.2011.01093.x.

Neal, J. C., I. Villanueva, N. G. Wright, T. Willis, T. J. Fewtrell and P. D. Bates (2012). 'How much physical complexity is needed to model flood inundation?' In: *Hydrological Processes* 26.15, pp. 2264–2282.

Néelz, S. and G. Pender (2013). *Benchmarking the latest generation of 2D Hydraulic Modelling Packages*. Tech. rep. Environment Agency.

Nesbitt, S. W. and A. M. Anders (2009). 'Very high resolution precipitation climatologies from the Tropical Rainfall Measuring Mission precipitation radar'. In: *Geophysical Research Letters* 36.15, n/a–n/a. ISSN: 00948276. DOI: 10.1029/2009GL038026. URL: http://doi.wiley.com/10.1029/2009GL038026.

Neteler, M., M. H. Bowman, M. Landa and M. Metz (2012). 'GRASS GIS: A multi-purpose open source GIS'. In: *Environmental Modelling & Software* 31, pp. 124–130.

O'Hara, K. J. and J. S. Kay (2003). 'Open source software and computer science education'. In: *Journal of Computing Sciences in Colleges* 18.3, pp. 1–7. URL: https://dl.acm.org/citation.cfm?id=771716.

Open Source Initiative (2007). *The Open Source Definition*. URL: https://opensource.org/osd (visited on 18/01/2018).

Palla, A., M. Colli, A. Candela, G. Aronica and L. Lanza (2016). 'Pluvial flooding in urban areas: the role of surface drainage efficiency'. In: *Journal of Flood Risk Management*. ISSN: 1753318X. DOI: 10.1111/jfr3.12246. URL: http://doi.wiley.com/10.1111/jfr3.12246.

Pankratz, R. H., M. R. Leblanc and A. Newcombe (1995). 'A Comparison of Dual Drainage Model Technique'. In: *Journal of Water Management Modeling*. ISSN: 22926062. DOI: 10.14796/JWMM.R183-23. URL: https://www.chijournal.org/R183-23.

Páramo, A. (2014). *Inundación histórica en la Ciudad de México*. URL: http://www.excelsior.com.mx/comunidad/2014/07/13/970607 (visited on 29/01/2018).

Paz, A. R., A. Meller and G. B. L. Silva (2011). 'Coupled 1D-2D hydraulic simulation of urban drainage systems: model development and preliminary results'. In:

Pedregosa, F., G. Varoquaux, A. Gramfort, V. Michel, B. Thirion, O. Grisel, M. Blondel, P. Prettenhofer, R. Weiss, V. Dubourg, J. Vanderplas, A. Passos, D. Cournapeau, M. Brucher, M. Perrot and É. Duchesnay (2011). 'Scikit-learn: Machine Learning in Python'. In: *Journal of Machine Learning Research* 12.Oct, pp. 2825–2830. URL: http://www.jmlr.org/papers/v12/pedregosa11a.html.

Pedrozo-Acuña, A., J. A. Breña-Naranjo and R. Domínguez-Mora (2014). 'The hydrological setting of the 2013 floods in Mexico'. In: *Weather* 69.11, pp. 295–302. ISSN: 00431656. DOI: 10.1002/wea.2355. URL: http://doi.wiley.com/10.1002/wea.2355.

Rawls, W. J., D. L. Brakensiek and N. Miller (1983). 'Green-Ampt infiltration parameters from soils data'. en. In: *Journal of Hydraulic Engineering* 109.1, pp. 62–70. ISSN: 0733-9429. DOI: 10.1061/(ASCE)0733-9429(1983)109:1(62).

Rico-Ramirez, M. A., S. Liguori and A. Schellart (2015). 'Quantifying radar-rainfall uncertainties in urban drainage flow modelling'. In: *Journal of Hydrology* 528, pp. 17–28. ISSN: 00221694. DOI: 10.1016/j.jhydrol.2015.05.057.

Ríos Elizondo, R., R. E. Ochoa E., M. Solano Gonzalez, G. Guerrero and G. Botas (1975). 'Aspectos tecnicos y administrativos de las obras del sistema de drenaje profundo'. In: *Memoria de las obras del sistema de drenaje profundo del Distrito Federal*. DDF. Chap. 3.

Rossman, L. A. (2010). *Storm Water Management Model User's Manual - Version 5.0*. Cincinnati, OH: US EPA - Water Supply and Water Resources Division.

Rubinato, M., R. Martins, G. Kesserwani, J. Leandro, S. Djordjević and J. D. Shucksmith (2017). 'Experimental calibration and validation of sewer/surface flow exchange equations in steady and unsteady flow conditions'. In: *Journal of Hydrology* 552, pp. 421–432. ISSN: 00221694. DOI: 10.1016/j.jhydrol.2017.06.024. URL: http://linkinghub.elsevier.com/retrieve/pii/S0022169417304286.

Saint-Venant, A. J. C. B. de (1871). 'Théorie du mouvement non permanent des eaux, avec application aux crues des rivières et à l'introduction des marées dans leurs lits'. In: *Comptes Rendus des séances de l'Académie des Sciences* 73, pp. 237–240.

Sampson, C. C., P. D. Bates, J. C. Neal and M. S. Horritt (2013). 'An automated routing methodology to enable direct rainfall in high resolution shallow water models'. In: *Hydrological Processes* 27.3, pp. 467–476. ISSN: 08856087. DOI: 10.1002/hyp.9515.

Sampson, C. C., A. M. Smith, P. D. Bates, J. C. Neal, L. Alfieri and J. E. Freer (2015). 'A high-resolution global flood hazard model'. In: *Water Resources Research* 51.9, pp. 7358–7381. ISSN: 00431397. DOI: 10.1002/2015WR016954. URL: http://doi.wiley.com/10.1002/2015WR016954.

Schmitt, T. G., M. Thomas and N. Ettrich (2004). 'Analysis and modeling of flooding in urban drainage systems'. In: *Journal of Hydrology* 299.3-4, pp. 300–311. ISSN: 00221694. DOI: 10.1016/j.jhydrol.2004.08.012.

Schmitt, T. G., M. Thomas and N. Ettrich (2005). 'Assessment of urban flooding by dual drainage simulation model RisUrSim'. In: *Water Science and Technology* 52.5.

Schuurmans, J. M., M. F. P. Bierkens, E. J. Pebesma and R. Uijlenhoet (2007). 'Automatic Prediction of High-Resolution Daily Rainfall Fields for Multiple Extents: The Potential of Operational Radar'. In: *Journal of Hydrometeorology* 8.6, pp. 1204–1224. ISSN: 1525-755X. DOI: 10.1175/2007JHM792.1. URL: http://journals.ametsoc.org/doi/abs/10.1175/2007JHM792.1.

Segond, M.-L., H. S. Wheater and C. Onof (2007). 'The significance of spatial rainfall representation for flood runoff estimation: A numerical evaluation based on the Lee catchment, UK'. In: *Journal of Hydrology* 347.1, pp. 116–131. ISSN: 00221694. DOI: 10.1016/j.jhydrol.2007.09.040.

Sen, D. (2013). 'Real-time rainfall monitoring and flood inundation forecasting for the city of Kolkata'. In: *ISH Journal of Hydraulic Engineering* 19.2, pp. 137–144. DOI: 10.1080/09715010.2013.787718.

Senior, M., R. Scheckenberger and B. Bishop (2018). 'Modeling Catchbasins and Inlets in SWMM'. In: *Journal of Water Management Modeling*. ISSN: 22926062. DOI: 10.14796/JWMM.C435. URL: https://www.chijournal.org/C435.

Seo, D.-J. (1998). 'Real-time estimation of rainfall fields using radar rainfall and rain gage data'. In: *Journal of Hydrology* 208.1-2, pp. 37–52. ISSN: 00221694. DOI: 10.1016/S0022-1694(98)00141-3. URL: http://linkinghub.elsevier.com/retrieve/pii/S0022169498001413.

Seyoum, S. D., Z. Vojinović, R. K. Price and S. Weesakul (2012). 'Coupled 1D and noninertia 2D flood inundation model for simulation of urban flooding'. In: *Journal of Hydraulic Engineering* 138.1, pp. 23–34.

Shrestha, N. K., B. De Fraine and W. Bauwens (2012). 'SWMM has become OpenMI compliant'. In: *Proceedings of the 9th International Conference on Urban Drainage Modelling, 4th-6th September, Belgrade, Serbia*.

Smith, J. A., M. L. Baeck, K. L. Meierdiercks, A. J. Miller and W. F. Krajewski (2007). 'Radar rainfall estimation for flash flood forecasting in small urban watersheds'. In: *Advances in Water Resources* 30.10, pp. 2087–2097. ISSN: 03091708. DOI: 10.1016/j.advwatres.2006.09.007. URL: http://linkinghub.elsevier.com/retrieve/pii/S0309170807000553.

Smith, J. A. and W. F. Krajewski (1993). 'A modeling study of rainfall rate-reflectivity relationships'. In: *Water Resources Research* 29.8, pp. 2505–

2514. ISSN: 00431397. DOI: 10.1029/93WR00962. URL: http://doi.wiley.com/10.1029/93WR00962.

United Nations (2014). *World Urbanization Prospects*. URL: https://esa.un.org/Unpd/Wup/.

Van Der Walt, S., S. C. Colbert and G. Varoquaux (2011). 'The NumPy array: a structure for efficient numerical computation'. In: *Computing in Science & Engineering* 13.2, pp. 22–30.

Velasco-Forero, C. A., D. Sempere-Torres, E. F. Cassiraga and J. J. Gómez-Hernández (2009). 'A non-parametric automatic blending methodology to estimate rainfall fields from rain gauge and radar data'. In: *Advances in Water Resources* 32.7, pp. 986–1002. ISSN: 03091708. DOI: 10.1016/j.advwatres.2008.10.004. URL: http://linkinghub.elsevier.com/retrieve/pii/S0309170808001760.

Vojinovic, Z. and D. Tutulic (2009). 'On the use of 1D and coupled 1D-2D modelling approaches for assessment of flood damage in urban areas'. In: *Urban Water Journal* 6.3, pp. 183–199. ISSN: 1573-062X. DOI: 10.1080/15730620802566877. URL: http://www.tandfonline.com/doi/abs/10.1080/15730620802566877.

Vojinović, Z. and M. B. Abbott (2012). *Flood risk and social justice : from quantitative to qualitative flood risk assessment and mitigation*. IWA Publishing, p. 563. ISBN: 1843393875.

Wilks, D. (2011). 'Forecast Verification'. In: *Statistical Methods in the Atmospheric Sciences*. Elsevier, pp. 301–394. ISBN: 978-0-12-385022-5. DOI: 10.1016/B978-0-12-385022-5.00008-7. URL: http://linkinghub.elsevier.com/retrieve/pii/B9780123850225000087.

Wilson, J. W. (1970). 'Integration of Radar and Raingage Data for Improved Rainfall Measurement'. In: *Journal of Applied Meteorology* 9.3, pp. 489–497. ISSN: 0021-8952. DOI: 10.1175/1520-0450(1970)009<0489:IORARD>2.0.CO;2. URL: http://journals.ametsoc.org/doi/abs/10.1175/1520-0450%7B%5C%%7D281970%7B%5C%%7D29009%7B%5C%%7D3C0489%7B%5C%%7D3AIORARD%7B%5C%%7D3E2.0.CO%7B%5C%%7D3B2.

Yu, D. and T. J. Coulthard (2015). 'Evaluating the importance of catchment hydrological parameters for urban surface water flood modelling using a simple hydro-inundation model'. In: *Journal of Hydrology* 524, pp. 385–400. ISSN: 00221694. DOI: 10.1016/j.jhydrol.2015.02.040.

Yu, D. and S. N. Lane (2006). 'Urban fluvial flood modelling using a two-dimensional diffusion-wave treatment, part 1: mesh resolution effects'. In: *Hydrologic Processes* 20.7, pp. 1541–1565.

Zambelli, P., S. Gebbert and M. Ciolli (2013). 'Pygrass: An object oriented python application programming interface (API) for geographic resources analysis support system (GRASS) geographic information system (GIS)'. In: *ISPRS International Journal of Geo-Information* 2.1, pp. 201–219.

Zevenbergen, C., A. C. Cashman, N. Evelpidou, E. Pasche, S. Garvin and R. Ashley (2010). *Urban Flood Management*. CRC Press. ISBN: 9781439894330.

Zhao, D.-q., J.-n. CHEN, Q.-y. TONG, H.-z. WANG, S.-b. CAO and Z. SHENG (2008). 'Construction of SWMM Urban Drainage Network Model Based on GIS'. In: *CHINA WATER AND WASTEWATER* 24.7, p. 88.

A Exported drainage values

Table A.1: Exported drainage node values in results vector maps.

Column	Description
cat	DB key
node_id	Name of the node
type	Node type (junction, storage, outlet etc.)
linkage_type	Equation used for the drainage/surface linkage
linkage_flow	Flow moving from the drainage to the surface ($m^3\,s^{-1}$)
inflow	Flow entering the node ($m^3\,s^{-1}$)
outflow	Flow exiting the node ($m^3\,s^{-1}$)
latFlow	SWMM lateral flow ($m^3\,s^{-1}$)
head	Hydraulic head (m)
crownElev	Elevation of the highest crown of the connected conduits (m)
crestElev	Elevation of the top of the node (m)
invertElev	Elevation of the bottom of the node (m)
initDepth	Water depth in the node at the start of the simulation (m)
fullDepth	*crownElev* – *invertElev* (m)
surDepth	Depth above *crownElev* before overflow begins (m)
pondedArea	Area above the node where ponding occurs (m^2)
degree	Number of pipes connected to the node
newVolume	Water volume in the node (m^3)
fullVolume	Volume in the node when *head* – *invertElev* = *crestElev* (m^3)

Table A.2: Exported drainage link values in results vector maps.

Column	Description
cat	DB key
link_id	Name of the link
type	Link type (conduit, pump etc.)
flow	Volumetric flow ($m^3\,s^{-1}$)
depth	Water depth in the conduit (m)
velocity	Average flow velocity ($m\,s^{-1}$)
volume	Water volume stored in the conduit (m^3)
offset1	Height above inlet node invert elevation (m)
offset2	Height above outlet node invert elevation (m)
yFull	Average water depth when the pipe is full (m)
froude	Average Froude number